https://dx.doi.org/10.1016/j.jechem.2022.08.027

Emerging Catalytic Materials for Practical Lithium-Sulfur Batteries

Fangyi Shi[1 #], Lingling Zhai [1#], Qingqing Liu[2], Jingya Yu,[1] Shu Ping Lau,[1*] Bao Yu Xia,[2*] Zheng-Long Xu[1,3,4*]

1. Department of Industrial and Systems Engineering, Department of Applied Physics, Research Institute of Advanced Manufacturing, the Hong Kong Polytechnic University, Hung Hom, Hong Kong, PR China.

2. Key Laboratory of Material Chemistry for Energy Conversion and Storage (Ministry of Education), Hubei Key Laboratory of Material Chemistry and Service Failure, School of Chemistry and Chemical Engineering, Huazhong University of Science and Technology (HUST), 1037 Luoyu Rd, Wuhan 430074, PR China.

3. State Key Laboratory of Ultraprecision Machining Technology, the Hong Kong Polytechnic University, Hung Hom, Hong Kong, PR China.

4. Hong Kong Polytechnic University Shenzhen Research Institute, Shenzhen, 518057, PR China

[#]These authors contributed equally to this work.

*Corresponding authors. Email: apsplau@polyu.edu.hk (S.P. Lau); byxia@hust.edu.cn (B. Y. Xia); and zhenglong.xu@polyu.edu.hk (Z.L. Xu)

Abstract: The high-energy lithium-sulfur batteries (LSBs) have experienced relentless development over the past decade with discernible improvement in electrochemical performance. However, a scrutinization of the cell operation conditions reveals a huge gap between the demands for practical batteries and those in the literature. Low-sulfur-loading, high electrolyte/sulfur (E/S) ratio and excess anodes for lab-scale LSBs significantly offset their high-energy merit. To approach practical LSBs, high-loading and lean-electrolyte parameters are required, which involve budding challenges of slow charge transfer, polysulfide precipitation and severe shuttle effect. To track these obstacles, the exploration of electrocatalyst to immobilize polysulfides and accelerate Li-S redox kinetics has been widely reported. Herein, this review aims to survey the state-of-the-art catalytic materials for practical LSBs with emphases on elucidating the correlation among catalyst design strategies, material structures and electrochemical performance. We also statistically evaluate the state-of-the-art catalyst-modified LSBs to identify the remaining discrepancy between the current advancements and the real-world requirements. In closing, we put forward our proposal for a catalytic material study to help realize practical LSBs.

Keywords: lithium-sulfur battery, catalytic materials, high sulfur loading, lean electrolyte

1. Introduction

Lithium-sulfur batteries (LSBs) have been considered promising alternatives to current lithium-ion batteries (LIBs) as the next-generation energy storage systems, due to the high abundance of sulfur stock and the exceptionally high theoretical energy density of 2567 Wh kg^{-1}.[1-3] However, the practical implementation of LSBs has been hampered by several fundamental challenges, namely, (i) the insulating nature of sulfur and Li_2S_2/Li_2S for low sulfur utilization and sluggish reaction kinetics, (ii) the dissolution and diffusion of lithium polysulfide intermediates (the so-called shuttle effect of LiPSs) for low Coulombic efficiency and self-discharge, (iii) the dendrite growth and parasitic reactions for lithium metal anodes for safety issues.[4] [5]

To mitigate the above obstacles, considerable efforts have been devoted to boosting the electrochemical performance since 2009, when Nazar and co-workers incorporated sulfur particles within conductive CMK-3 porous carbon.[6] The efforts include the impregnation of sulfur within conductive and porous carbon materials for improved sulfur utilization, the modification of electrolyte for enhancing ionic conductivity and suppressing polysulfide diffusion, the engineering of interlayer or/and separator for protecting Li metal anode, and the upgrade of binders, current collectors and cell configurations. Great advances have been witnessed, for example, LSBs can cycle for 2000 times,[7, 8] at ultra-high rate 40C,[9, 10] and present a high capacity of 1200 mAh g^{-1}.[11, 12] However, most of the reported studies were performed using coin cells under ideal conditions (*i.e.*, excess electrolyte, low sulfur loading and uncontrolled Li anode).[13] Although these parameters are conductive for fundamental research, the excessive electrolyte and limited active component would not only offset the high-energy merit for LSBs but also conceal the real challenges. [14, 15] For example, when the mass loading and electrolyte/sulfur ratio (E/S ratio) of a single-atom Fe-N_2 mediated sulfur cathode were increased from 2.0 mg cm^{-2} and 15 μL mg^{-1} to 5.75 mg cm^{-2} and 7.35 μL mg^{-1}, respectively, the cycle life dramatically shrank from 2000 to 55 cycles.[8] To promote practical LSBs, parameters of the sulfur loading and electrolyte amount shall not be overlooked. [14, 16-19]

Transparent calculations of the energy density for practical LSBs suggest values for the high-sulfur-loadings (≥8 mg cm^{-2}), high sulfur content (≥70 wt%), and low E/S ratios (≤3 μL mg^{-1}).[14] In the actual working condition,

however, the reversibility and reaction kinetics in LSBs become greatly restricted due to several emerging issues, namely, (i) the saturation and precipitation of LiPSs, (ii) the exacerbated ion diffusion kinetics, (iii) poor electrode wettability, and (iv) the rapid failure of Li metal anode.[20] The development of catalytic materials has been demonstrated promising to regulate the Li-S redox process and prevent LiPS accumulation, thus alleviating the "dead sulfur" formation and slow conversion kinetics in practical LSBs.[21] Fig. 1a shows the exponential increase of publication numbers related to catalyst materials for high performance LSBs. The catalysts reported so far (Fig. 1b) can be classified into conventional catalytic materials (*e.g.*, metal oxides, metal sulfides, phosphates) and the emerging ones (*e.g.*, single-atoms catalyst, heterostructure catalyst, catalysts with defects). The former has been far-reaching and extensively studied to immobilize and catalyze LiPSs in ideal conditions, while the latter appeared freshly to regulate the Li-S chemistry under high-sulfur-loading and lean-electrolyte conditions.[22-25]

Despite several previous reports discussing the working mechanisms and nanostructures of budding catalytic materials in LSBs, they have not covered two critical issues: (i) the design principles for emerging catalysts in practical LSBs and (ii) the residual gap between the high-profile catalyst-modified LSBs in laboratory and the requirements from the real-world. In this review, we are dedicated to primarily discussing these aspects. The important parameters and attendant issues for practical LSB batteries will be initially survived. Then, the design principles for high-efficiency catalysts will be discussed on base of their dimensions. Subsequently, we will focus on analyzing the electrochemical performance of emerging catalysts in high-loading and lean-electrolyte LSBs. Before proposing the conclusion and perspectives at last, a statistical analysis of related papers published in the last 5 years (2018-now) will be conducted to project the demonstrated achievements and remaining challenges for advanced catalysts in LSBs.

2. Requirements and challenges for practical lithium-sulfur batteries

A typical LSB consists of a sulfur/carbon cathode, a lithium metal anode and a separator filled with organic electrolyte (*i.e.*, 1M LiTFSI in DME/DOL) inserted in between. During discharging, the sulfur is converted to Li_2S at a moderate voltage of 2.2 V (vs. Li^+/Li) with a high theoretical capacity of 1675 mAh g^{-1}, resulting in an

overwhelmingly high theoretical energy density of 2567 Wh kg^{-1}. Unfortunately, the practical energy density values are much lower, due to the incomplete utilization of insulating sulfur, the excessive electrolyte and Li metal anode, and other inactive components (*i.e.*, binder, current collector and separator). To estimate the key parameters affecting the energy density of LSBs, a formulation for energy density calculation was newly proposed by Zhou *et al.*[1]:

$$\text{Energy density} = 2567\ \text{Wh kg}^{-1} \times R_{weight} \times R_{energy} \quad (1)$$

where R_{weight} and R_{energy} are the weight ratio of active materials and energy utilization ratio. They can be further described as:

$$R_{energy} = \frac{C_{sulfur}}{1675\ \text{mAh g}^{-1}} \times \frac{V_{cathode}}{2.2V} \quad (2)$$

$$R_{weight} = \frac{\frac{M_{Li_2S}}{M_S} \times m_{sl} \times (1\text{-}R_{package})}{\frac{m_{sl}}{R_{cathode}} + \frac{m_{Al}+m_{Cu}}{2} + m_{separator} + \rho_E \times R_{E/S} \times m_{sl} + \frac{2M_{Li}}{M_S \times R_{N/P} \times m_{sl}}} \quad (3)$$

where C_{sulfur} and $V_{cathode}$ are the specific capacity of sulfur and average cell voltage. M_{Li}, M_s and M_{Li2S} represent the molar weight of lithium, sulfur, and Li_2S. $R_{cathode}$, $R_{E/S}$ and $R_{N/P}$ illustrate the weight ration of sulfur in the cathode, the ratio of electrolyte to sulfur loading (E/S, μL mg^{-1}) and the ratio of the theoretical areal capacity of Li anode to that for sulfur cathode, respectively. m_{sl}, $m_{separator}$, m_{Al} and m_{Cu} are the areal masses of sulfur, separator, Al current collector, Cu current collector. ρ_E refers to the density of electrolyte. Equation (3) can be simplified by inputting the value of parameters that are commonly used in practical cells (M_{Li}=6.941, M_s=32.065, M_{Li2S}=45.95, $R_{cathode}$=10 wt%, $R_{N/P}$=2, $m_{separator}$= 1.1 mg cm^{-2}, m_{Al}=2.7 mg cm^{-2}, m_{Cu}=0 for Li metal as the current collector, ρ_E= 1.1 g ml^{-1}):

$$R_{weight} = \frac{1.433 \times m_{sl} \times 0.9}{2.35 + (1.11 + 1.1 \times R_{E/S} + 0.433 \times 2) \times m_{sl}} \quad (4)$$

According to the above equations, the relationship among R_{weight}, m_{sl} and $R_{E/S}$ can be illustrated in Fig. 2a. It implies that decreasing the E/S ratio is one of the inevitable avenues to approach high R_{weight} and overall energy densities. Most of the promoted performances in literature however are based on high E/S ratios (> 10 μL mg^{-1}) [14] and low sulfur loadings (<2.0 mg cm^{-2}).[26] Flooded electrolyte indicates the capability to dissolve more LiPSs for decent specific capacities, but with a penalty to the overall energy density.[27-29] Gupta *et al.*[30] calculated that the E/S ratio should be lower than 5 uL mg^{-1} assuming a 100% sulfur utilization with a m_{sl} of 10

mg cm^{-2} (Fig. 2b), if Li-S cells are designed for the 500 Wh kg^{-1} target. Setting 500 Wh kg^{-1} and 400 Wh kg^{-1} as boundaries, Zhao *et al*.[14] plotted the relationship between the E/S ratio and sulfur loading of Li-S pouch cells. The m_{sl} with 5 mg cm^{-2} and E/S ratio of 4 μL mg^{-1} can promise an energy density of 400 Wh kg^{-1}, and an energy density of 500 Wh kg^{-1} needs m_{sl} = 6 mg cm^{-2} and E/S ratio = 2.5 μL mg^{-1} (Fig. 2c).

Above calculations define the boundaries of sulfur loading and E/S ratio to achieve practical LSBs. With the traditional challenges of insulating active materials, volume expansion and polysulfide diffusion being addressed, new problems emerge in lean-electrolyte and high-loading LSBs and become the bottleneck to approach appreciable cell performance.[27, 31, 32] It is thus necessary to define the emerging challenges first before elaborating the catalytic material design strategies for the development of practical LSBs. The major problems are listed as follows:

(1) Highly concentrated LiPSs: In actual working conditions, the massive LiPSs would interact with free solvents through solvation or forming clusters with lithium slats, thus resulting in significantly improved viscosity and decreased ionic conductivity. The large viscosity will aggravate the electrolyte/electrode interfacial resistance, which induces kinetic obstructs to the sulfur redox reactions on catalyst surfaces.[33, 34] In addition, the large polarizations caused by highly concentrated LiPSs in limited electrolyte would manifest poor rate performance and low sulfur utilizations. If the LiPS concentration exceeds its saturation ceiling, cell failure may occur. Therefore, the highly concentrated LiPSs shall be taken seriously as an emerging challenge.

(2) Chemical reactions of LiPSs: In ideal conditions, the long-chain LiPSs dissolved in the ether-based electrolyte are ready to be electrochemically reduced into solid lithium sulfides, along with marginal chemical disproportion among sulfur species (*i.e.*, $S_8 + Li_2S_4 \leftrightarrow Li_2S_6$). However, in low E/S ratio and high sulfur loading conditions, the chemical reactions become more dominant with high LiPS concentrations, causing premature precipitation of LiPSs and aggregation of solid reaction products. These insulating precipitates tend to lose electrical contact from conductive substrate during cycling. Consequently, a new balance between the chemical and electrochemical pathways will be constructed in practical LSBs. In addition, the concentration-driven LiPSs diffusion between the anodes and cathodes will be augmented to aggravate the parasitic reaction on the Li metal anode side.[35] The

enhanced LiPS chemical reactions, which are trivial in ideal conditions, become another important problem in practical LSBs requiring new insights and effective regulation strategies.

(3) Low sulfur utilization: Sulfur utilization is closely related to the charge transfer kinetics at the electrolyte/sulfur/carbon interfaces. In excessive electrolytes, sulfur particles can be accessible to conductive carbon with large surface areas and LiPS mediators. However, in practical LSBs, high concentration sulfur species would be away from conductive surfaces. Due to the limited electrolyte amount, sulfur particles may also be isolated from the electrolyte, thereby the charge transfer pathway is blocked without sulfur redox reactions (Fig. 2d).[36] During charging, the Li_2S precipitates require higher activation energies without diluting LiPSs mediator, resulting in low utilization of the active materials.[37] Low sulfur utilization has been widely observed with shortened discharge plateaus, thus how to maintain the high capacities under rigorous conditions is the third major challenge.

(4) Unstable lithium metal anode: The degradation of lithium metal anode is usually masked in Li-S coin cell tests due to the excess amount of lithium metal and electrolyte in ideal conditions (*i.e.*, N/P ratio of above 150 and E/S ratio of above 20 uL mg^{-1}). However, in practical LSBs, the unstable lithium metal can cause rapid capacity degradation and battery failure, due to the following emerging issues: (i) the meager electrolyte is easy to deplete from parasitic reactions among the electrolyte, Li metal and polysulfides, (ii) the concentrated LiPSs render serious Li metal corrosion and surface passivation, and (iii) limited excess Li metal in low N/P ratio condition cannot withstand the repeated corrosion or capacity loss during cycles.[38] Therefore, preserving the excellent reversibility and stability of thin lithium metal anode shall not be overlooked for practical LSBs.

In order to overcome these emerging problems, optimizing cathode architecture, electrocatalyst, electrolyte structures, and Li anode protection have been considered necessary.[27, 39] [40] Among them, the development of novel electrocatalyst is regarded as the key to solving the slow kinetics and unstable cycling problems by effectively regulating the Li-S chemistry.[41] High sulfur loading and low E/S ratio inevitably bring highly concentrated LiPSs. Selective catalysts were reported to promote the conversion of soluble LiPSs to solid Li_2S_2/Li_2S, meanwhile, decelerate the reaction rate from sulfur to Li_2S_8, thus preventing the accumulation of

LiPSs in bulk electrolyte [42]. The catalytic functions not only promote the sulfur utilization in practical conditions but also stabilize the Li metal anode by alleviating the LiPSs concentration gradient from the cathode to the anode [43]. In addition, catalyst materials showing strong absorption for LiPSs can suppress the chemical disproportionation reactions in battery storage and operation conditions [44, 45]. Thus, we will focus on examining the catalytic material strategy for practical LSBs as follows.

3. Design principles for advanced catalysts in Li-S batteries

Due to the soluble Li_2S_4 being reduced to Li_2S_2/Li_2S is a rate-limiting step, the concentration of LiPSs will increase around the cathode to exacerbate the shuttle effect. Electrocatalysts can take the privilege to entrap polysulfides and accelerate the redox reaction kinetics for alleviating the polysulfide accumulation and suppressing the shuttle effect. The concept of 'catalyst materials' has been reported in LSBs working in ideal conditions by serving as cathode matrixes, electrolyte additives, and separator modifiers. The general requirements of catalysts include the strong LiPSs adsorption ability, the abundant catalytically active sites and excellent electronic/ionic conductivities.[46] Catalytic materials do not work alone, they are usually embedded in conductive and highly porous carbon materials for uniform dispersion of catalyst particles with rapid electron transfer pathways.[47-49] For example, 1T MoS_2 nanosheets were integrated with 3D graphene network to maximize the aspect ratio of the active sites.[50] Despite the long-term and in-depth progress reported for conventional catalysts, such as metal sulfides, nitrides, oxides and carbide compounds, some emerging catalytic materials attracted increasing attention to meet the rigorous working conditions in practical LSBs. To avoid duplicating the reviews of developed catalysts, we will focus on the state-of-the-art catalysts in practical LSBs, such as single atom catalysts, defective site catalysts and quantum dot catalysts. Before elaborating the catalytic materials and the enhanced electrochemical performance in LSBs, in-depth understandings of the catalyst design rules are discussed.

3.1 Abundant active sites

Active sites in catalysts can not only immobilize the soluble LiPSs but also provide nucleation sites for Li_2S_2/Li_2S deposition. For improving the activity of electrocatalyst, there are two main methods, including increasing the active site density and boosting the activity of each site.[51]

Although the number of active sites possesses positive correlation to the catalyst loading, a large proportion of electrochemically inert catalysts can impede the mass/charge transport and sacrifice the energy density of LSBs. Downsizing bulk catalysts into nanodots even single atoms can significantly enlarge the exposed surface areas for abundant catalytic sites. A representative example to this concept is the preparation of black phosphorus quantum dots (BPQDs, ~2.5 nm × 4.5nm) from BP flacks (6.1 nm × 800 nm) [52]. With enlarged catalytically active edge areas (Fig. 3a), the chemical affinity to soluble LiPSs (Fig. 3b) and Li_2S deposition capacity (Fig. 3c) were significantly enhanced by using BPQDs. Similarly, the catalytic activity of MoS_2 was also maximized by synthesizing 1T nanodots (NDs).[53] In the presence of a small amount of MoS_2 NDs (3 wt% of the electrode), Li-S cells presented an area capacity of 9.3 mAh cm^{-2} after 300 cycled with a high m_{sl} of 12.9 mg cm^{-2} and a low E/S ratio of 4.6 μL mg^{-1}. Constructing interface or grain boundaries is another effective strategy to amplify the active site densities. For example, Yang *et al*.[46] designed a SnO_2/Mo_2N heterostructure with SnO_2 NDs anchoring on Mo_2N microbelt. The numerous SnO_2/Mo_2N interfaces indicated a great synergistic effect with strong chemical affinities to LiPSs and the ability to guide the three-dimensional (3D) deposition of Li_2S (Fig. 3d). A homogeneous Ti_3C_2 MXene nanodot/nanosheet structure was also reported [54] to offer rich active sites at the edge areas and interfaces.

Atomic engineering is another plausible strategy to boost the active site densities. For example, 2H MoS_2 nanosheet displays catalytic activity on the limited edge areas instead of the large basal plane.[55] By creating sulfur atomic deficiencies, the MoS_{2-x} basal plane was obviously activated.[56] With the increased number of active sites and improved catalytic efficiency, the MoS_{2-x}/rGO/S cathode displayed a much higher rate capacity (826.5 mAh g^{-1} vs. 473.3 mAh g^{-1} at 8 C) and cyclability than MoS_2/rGO/S cathode (capacity retention of 70.7% vs. 55.7% after 150 cycles at 0.5C). Zhou *et al*.[57] proposed to control the exposed crystal facet to intensify the catalytic activity of Co_2P. The absorption or activation of reactant molecules was prone to happen at the exposed

surface crystal plane with low coordination saturations and reaction activation energies. The consequences proved that the increase of Co_2P (211) lattice planes exhibited higher adsorption and catalytic abilities to LiPSs than with the (121) plane. Thus, improved battery performance was obtained with the facet engineered Co_2P catalyst.

In order to improve the activity of each catalytic site, defect engineering has been proposed to adjust the local electronic structures. Shen *et al*.[58] rationally designed nitrogen (N) vacancies on Ni_3N to form $Ni_3N_{0.85}$ (Fig. 3e). By introducing N vacancies, the *d*-band center of catalysts was adjusted with lengthened Ni-Ni bonds in $Ni_3N_{0.85}$ compared to Ni_3N. It favored the Ni bridging sites to form a strong affiliation with sulfur species, therefore, the LiPS anchoring capability for $Ni_3N_{0.85}$ is higher than Ni_3N (Fig. 3f). In addition, the $Ni_3N_{0.85}$ displayed higher electron density for Ni-S bonds (Fig. 3g), suggesting a strong covalence between the terminal S in LiPSs and the Ni atoms on $Ni_3N_{0.85}$ surface, thereby accelerating the conversion of polysulfides. Besides introducing vacancies, heteroatom doping is another method to activate the catalytic sites. For example, Lin *et al*.[59] reported Co and P co-doped MoS_2 as a powerful catalyst. The dopants created an electron-rich environment and facilitated the S-S bonds break for LiPS conversion. Phase transition engineering was also demonstrated effective in enhancing the activity of catalytic materials. When the crystal phase is adjusted, the tailored surface may exhibit favorable adsorption and charge state to regulate the Li-S redox.[60] The mediocre 2H MoS_2 phase transferring to a sublime 1T phase with better conductivity and catalytic capability is a good example of this strategy.[50] Similarly, the LSBs using 1T $MoSe_2$ achieved better electrochemical performance than in 2H $MoSe_2$ due to the superior catalytic activities and conductivity for the 1T phase.[61] The heterostructure interface can reconfigure the Fermi-level energies and local electronic structures, thus potentially offering synergistic effects in catalytic activities. For example, TiN-TiO_2 heterostructure was reported performing better catalytic performance than TiN or TiO_2 alone.[62]

In summary, both intensifying the exposed active sites and boosting the catalytic activity of individual site are effective to amplify the catalytic capability for emerging catalytic materials. More importantly, these strategies can work synergistically to further reinforce the catalytic efficiency. In particular, defect and heterostructure

engineering are promising to enhance the intrinsic activity but also create more active sites simultaneously. The promoted catalytic activity allows the usage of the tiny amount of catalysts to achieve practical high-energy LSBs.

3.2 Multifunctional capability

The Li-S reactions involve complicated "solid-liquid-solid" phase evolutions and "sulfur-LiPS-Li_2S" chemical changes. It is thereby difficult for a single catalyst to properly regulate the multi-step redox reactions simultaneously. To this end, multi-functional catalytic materials are desired. There are three main objectives for multi-functional catalysts design: (i) for smooth "immobilization-diffusion-conversion" of LiPSs, (ii) for bidirectional catalysis during charging and discharging, and (iii) for stabilizing the Li metal anode.

To alleviate the shuttle effect and increase the sulfur utilization for high-loading LSBs, rapid diffusion and conversion of trapped LiPSs on the surface of catalysts are necessary. A variety of catalysts enabling "immobilization-diffusion-conversion" of LiPSs have been developed.[63] The TiO_2-MXene heterostructure is a representative example,[64] which integrated the strong LiPSs absorptivity of TiO_2 nanoparticles and the rapid LiPSs conversion capability of MXene. The advanced LSBs showed sustainable cyclability at high sulfur loadings, *i.e.*, the capacity retention of 93% after 200 cycles at a high sulfur loading of 5.1 mg cm^{-2}. It was reported that the transformation of polysulfides from high order to low order is much faster than the reduction of Li_2S_4 to solid Li_2S_2/Li_2S. The kinetic mismatch would cause saturation of LiPSs on the surface of catalysts, thus homogenizing the conversion kinetics is critical to alleviate the accumulation of LiPSs. Hua *et al*.[65] reported that the In_2O_3 catalyst could selectively decelerate the conversion from sulfur to LiPSs while accelerating the reduction of Li_2S_4 to Li_2S, thus preventing the accumulation of LiPSs in the electrolyte and suppressing the shuttle effect.

Catalysis of deposited Li_2S to LiPS and sulfur is of equal importance to achieve high sulfur utilization and Coulombic efficiencies. In this regard, Chen *et al*.[66] reported a Ni/Zn dual-doped $CoSe_2$ catalyst displaying great catalysis abilities in both the reduction and oxidation processes in LSBs. In particular, the Ni dopant shortened the Co-S bond and extended the S-S bonds, thus facilitating the LiPSs reduction to Li_2S_2/Li_2S during discharging. Whereas, the Zn dopant induced elongated Li-S bonds to lower the energy barriers for Li_2S decomposition during charging. Density of states (DOS) curves indicated the best electric properties for the

Ni/Zn-doped $CoSe_2$ among pristine, Ni-doped, Zn-doped and co-doped $CoSe_2$ samples (Fig. 4a), which benefited the fast charge transfer and reaction kinetics. In addition, the charge number adjusted Co element exhibited a stronger chemical affinity to LiPSs (Fig. 4b). Therefore, the co-doped $CoSe_2$ exhibited excellent bi-directional catalysis properties. The intriguing "immobilization-adsorption-conversion" and the "bidirectional" catalytic properties can be integrated in heterostructures. Taking TiO_2-Ni_3S_2 as an example,[67] the TiO_2 can provide strong LiPSs anchoring and diffusion surfaces for rapid conversion on Ni_3S_2, while the oxidation of Li_2S could be catalyzed by TiO_2 and Ni_3S_2 simultaneously.

Besides the cathode side, stabilization of the lithium metal anode is also necessary for durable LSBs. Architecting bifunctional separators have attracted attention in this regard. The modified separator is designed to simultaneously regulate Li-ion flux for uniform and dense Li metal deposition at anodes and to hunt and reuse the LiPSs at cathodes.[68-70] Metal−organic frameworks (MOFs) constituted by organic ligands and inorganic metal ions present tunable open channels for Li-ion redistribution and numerous metal sites for LiPS entrapment and conversion. Thus, MOFs are regarded promising to modify separators.[68, 69] Hong *et al*.[69] reported a Ce-MOF/carbon nanotube (CNT) coated separator in LSBs (Fig. 4c). The CNTs network provided the conductive pathway to reuse the LiPSs anchored by Ce-MOF particles. The coordination-unsaturated Ce (IV)-cluster nodes on Ce-MOF are useful to accelerate the reduction of LiPSs. More importantly, the Ce-MOF/CNT-modified separator offered uniform electric field and ion diffusion channels to prevent Li dendrites formation, ensuring smooth and dense Li metal surfaces after 800 cycles. Analogically, Li *et al*.[71] prepared a bifunctional separator using single-Co-atom decorated MOF nanosheets. The Co atoms coordinated with oxygen (Co-O_4 moieties) can anchor soluble LiPSs by Lewis acid-based interaction. The O atoms presented a strong affinity to Li-ion, which can homogenize the Li-ion flux to avoid dendrite formation. The MOF-modified separators possessing high Yong's modulus could further impede the Li dendrite growth (Fig. 4d).

To sum up, the redox reactions in LSBs are multi-step, multi-phase and multi-component involved, and each conversion step will significantly influence the overall battery performance. The design of catalytic materials should comprehensively consider the specific conversion kinetics, the local environment of LiPSs and the stability

of Li metal anode. Multifunctional catalysts integrating the merits of individual catalysts are therefore more desirable.

3.3 Synergy of functional components

As discussed above, the catalytic property is highly dependent on the nature of active sites. Combining two or more catalysts to integrate multiple functionalities could effectively improve the overall catalytic performance.[72] For instance, metal oxides with high polarities can strongly absorb LiPSs, but their low conductivities limit the catalytic efficiency, whereas metal nitrides own great conductivity but fail to efficiently absorb LiPSs.[41] In response, heterostructure catalysts have been reported, such as TiO_2-TiN,[62] NiO-$NiCo_2O_4$,[73] VTe_2-MgO,[74] MoS_2-MoN[75], in which some components function to anchor LiPSs and others to accelerate redox kinetics. The profound challenge in constructing heterostructures is the compatibility of each component, which means it is not universal to form a heterointerface for different materials. To mitigate this issue, different catalyst materials can be directly loaded into the same matrix without forming heterojunctions. A distinctive example of this idea was reported by Zhao *et al*.[76] to prepare highly oriented porous carbon decorated with ZnS nanoparticles and Co-N-C single atom (Co-SACs) (Fig. 5a). The LiPSs could be bonded by the Co metal atoms through Lewis acid interaction and ZnS through polar-polar interaction (Fig. 5b). Thus, the double-ended binding sites ensured the strong binding strength and fast reaction kinetics.

On the way to constructing synergetic catalyst materials, fundamental insights into the working mechanisms of each catalytic component are imperative. Theoretical modeling has been regarded as a game-changing approach allowing intensive illustrations of the electronic, catalytic and chemical properties of potential catalyst components.[77] This information can provide profound guidance toward the design of powerful catalyst. For example, Zhou *et al*.[78] compared the Li_2S decomposition energy barriers, binding energies, and lithium diffusion rates of various metal sulfides (VS_2, CoS_2, TiS_2, FeS_2, SnS_2, and Ni_2S_3) by density functional theory (DFT) simulations. VS_2 indicated the lowest Li-ion diffusion energy barriers, resulting in the lowest activation voltage for Li_2S oxidation on VS_2 in real batteries. To select proper SACs, Zhou *et al*.[79] calculated the Li_2S decomposition barriers, Li-ion diffusion barriers and LiPSs binding energies of various SACs (*i.e*., Fe, Mn, Ru,

Zn, Co, Cu, V, Ag) decorated on N-doped graphene (Fig. 5c-e). Despite the similar Li-ion diffusion kinetics (Fig. 5c), SAV@NG stood out by exhibiting the smallest Li_2S deposition barrier (Fig. 5d) and the largest binding energy with LiPSs (Fig. 5e). Consequently, LSBs with SAV@NG sulfur cathodes showed the strongest absorption to Li_2S_6 (Fig. 5f) and the highest capacity retention after 400 cycles at 0.5 C (Fig. 5g). The hybridization between the *p* orbital of sulfur species and *d* orbitals of SAC is another important indicator of catalytic efficient. Han *et al*.[77] found that low atomic number transition metals, like Ti, displayed more effective *d-p* hybridization with fewer anti-bonding states than Sc, Ti, V, Cr, Mn, Fe, Co, Ni, and Cu (Fig. 5h), which can lower the deposition and decomposition energy barriers for Li_2S. By virtue of 1wt.% single-atom Ti catalyst on sulfur/carbon composites, the cathode exhibited remarkable electrochemical performance at a sulfur loading of 4 mg cm^{-2} (Fig. 5i). Surface terminal groups are also essential for the catalytic activities. Wang *et al*.[80] studied the catalytic and absorption ability of Ti_3C_2 with different functional groups (*i.e.*, N, P, O, S, F, and Cl). It revealed that S and O groups can adjust the LiPSs absorption energies of Ti_3C_2 to be neither too strong for LiPSs reduction chemically nor too weak for LiPSs diffusion in the electrolyte.

In short, the synergetic methodology of integrating different catalytic materials or sites in one system would be effective in achieving the simultaneous LiPSs immobilization and conversion, thereby figuring out the intricate Li-S chemistry. With the exposition of novel material fabrication processes and the utilization of simulation tools, the material integration for reasonable management of Li-S reactions is believed to be feasible and promising.

4. Emerging catalysts in high-loading and lean-electrolyte Li-S Batteries

After intensive discussions on the design principles for powerful catalytic materials for LSBs, we will put efforts into surveying the budding catalytic materials reported in the last 5 years. It is noted again that the investigations of electrocatalyst in LSBs appeared years ago, and tremendous catalytic materials have been studied in ameliorating the battery performance. However, only recently has been more attention paid to developing highly efficient, light weight and atomic-level catalytic materials for high-loading and lean-electrolyte LSBs. The nascent catalyst materials can be primarily categorized into single metals, defective sites, quantum dots/nanodots

and heterostructures in view of their dimensions. The correlations between the nature of catalytic materials and the electrochemical behaviors in advanced LSBs will be examined in this section.

4.1 Single atom catalysts

Compared to the traditional bulk catalysts, single-atom catalysts (SACs) with atomic size level active sites possess near 100% atom utilization efficiency. Moreover, the unsaturated metal species with unique electronic structures and well-defined catalytic centers show outstanding catalytic properties in LSBs. The intriguing SACs have been increasingly reported in amending the sulfur cathodes, lithium anodes, and separators in LSBs (Fig. 6a).[30] [81] On the cathode side, SACs mainly function two roles, namely, anchoring LPSs through Lewis acid-base interactions and promoting the reaction kinetics.[76] The SACs are also verified to regulate rate-limiting steps between the liquid LiPSs and solid Li_2S_2/Li_2S by lowering the phase transition energy barriers. The common strategy to obtain uniformly distributed SACs is coordinating them with non-metal groups (such as N, and O) on carbon substrates.[82, 83] For example, Du *et al*. [84] prepared single-atom Co on nitrogen-doped graphene (Co-N/G). The Co-N/G could effectively absorb Li_2S_6 and lower the Gibbs free energy changes for Li_2S_4 reduction to Li_2S_2/Li_2S (Fig. 6b). The Li_2S decomposition on the Co-N/G substrate was also facilitated (Fig. 6c). In the presence of Co-N/G catalyst, the high-loading Li-S cell (m_{sl}= 6.0 mg cm^{-2}) presented capacity retentions of above 5 mAh cm^{-2} after 100 cycles (Fig. 6d). To enhance the affinity with LiPSs, Zhang *et al*.[85] prepared single-atom nickel (Ni)-nitrogen-doped graphene (Ni@NG) catalyst. The Ni-N_4 structure played a role in anchoring the LiPSs and boosting the Li-S conversion kinetics during cycling. At the discharge plateau of 2.1 V, the LiPSs will form Ni-S bonding and Lewis acid-base interaction between the *d* orbital of the Ni atom and the LiPSs anions. Together with the strong electrostatic interaction between N atoms in graphene and Li-ion, the Ni-N_4 could effectively accommodate LiPSs. The resultant LSB can maintain a reversible capacity of 503 mAh g^{-1} after 100 cycles at 1.0 C with a high m_{sl} of 6.0 mg cm^{-2}. Non-carbon substrates have also been integrated with SACs. Lu *et al*.[86] used g-C_3N_4 support to improve the SACs loading. A remarkable 8.5 wt% of single-atom Fe on SAFe@g-C_3N_4 was obtained due to the rich N-doping on C_3N_4. The SAFe@g-C_3N_4-sulfur cathodes performed a 90% capacity retention after 200 cycles at an extremely low E/S ratio of 3.8 μL mg^{-1}.

To enable uniform deposition of Li metal, SACs-modified coating/protective layer on Li metal or SACs-decorated separators have been studied in LSBs.[87] For example, Song *et al*.[88] prepared a Janus separator with one side coated by single-atom Zn/N-doped carbon and another side by the anionic metal-organic framework (denoted as SAZ-AF in Fig. 6e). The single-atom Zn catalyzed the rapid transformation of LiPSs, thus preventing the LiPS shuttling and corroding the Li metal anode. The anionic MOF coating induced uniform Li-ion reduction without dendrite formation. As a consequence, the Li-S cell inserted with SAZ-AF Janus separator stably cycled over 100 times with a capacity retention of 564.7 mAh g^{-1} at 2 C (Fig. 6f). Similarly, the cell with 2D MOF Co-decorated separator retained a reversible capacity of 5.1 mAh cm^{-2} at 0.5C with a high m_{sl} of 7.8 mg cm^{-2} [71].

SAC-modified host can also efficiently protect the Li metal anode and improve the reversibility of Li plating/stripping. Liu *et al*.[89] prepared a CoN_x-doped graphene (CoNC) matrix for ultrastable Li metal anode. The CoNC showed a higher absorptivity to Li-ion than N-doped graphene, referring to superior lithiophilicity, thus lower nucleation overpotential was observed for Li plating on the CoNC substrate. The CoNC electrode displayed dendrite-free cycling at 2.0 and 5.0 mA cm^{-2} for 200 cycles. Zhai *et al*.[89] synthesized a series of single-atom M (SAM, M=Ni, Pt, Cu) on the N-G matrix as Li metal host. The SAM can regulate the Li nucleation and deposition to avoid the formation of Li dendrite. The single-atom Fe in a N-doped carbon can provide lithiophilic site to decrease the Li nucleation overpotential and promise Li plating/stripping stability.[90] Apart from carbon matrix, SACs has also been introduced other substrates, like MXene.[91] [92] The above examples demonstrate that SACs can provide lithiophilic nucleation sites, which offers opportunities to stabilize the limited Li metal in practical LSBs.

4.2 Defective site catalysts

Despite the great achievements for SAC-modified LSBs, it is still challenging to synthesize high-loading SACs in high-yielding and low-cost manners. The requirement of elaborative experimental processes for SACs preparation also stimulates the exploration of other atomic-level catalytic materials. Defect engineering is a promising methodology, which can effectively tune the electronic conductivity and ionic diffusion of the catalysts by narrowing band gaps and enriching the energy levels.[47] In addition, polarity and catalytic activity can be

introduced to nonpolar materials by defect engineering, leading to enhanced absorptivity and catalysis of LiPSs. More importantly, defective sites can be simply accessed on a large scale. Taking these advantages into account, defective site catalysts have been profoundly studied, which can be classified as heteroatom doping, vacancy engineering and synergy of them.

Heteroatom doping includes metal element doping (*i.e.*, Mo, Co, Ni, Zn) [59, 93-95] and metal-free element doping (*i.e.*, P, N, O) [93, 96, 97]. For metallic atom doping, Feng *et al*.[93] reported Mo-doped cobalt borides amorphous (Co_7Mo_3B) displaying great electronic conductivities, strong LiPSs affinity, and excellent catalysis ability. In the LSV curve corresponding to the Li_2S precipitation process, the Co_7Mo_3B electrode presented an earlier and higher current peak than that for the CoB (Fig. 7a). For the Li_2S dissolution process, the Co_7Mo_3B/Li_2S electrode delivered higher dissolution capacity and current responses than CoB (Fig. 7b). These results illustrated that Co_7Mo_3B bi-directionally catalyzed the reduction and oxidation of polysulfides. To investigate the application of Co_7Mo_3B in practical LSBs, Li-S pouch cells with a high m_{sl} of 3.45 mg cm^{-2} and a low E/S ratio of 6 μL mg^{-1} were assembled and maintained high capacity retention after 20 cycles at 0.1 C (Fig. 7c). Co atom was also doped in transition 2D metal sulfides to enhance the catalytic performance. For example, Liu *et al*.[94] introduced a Co-doped MoS_2 (Co-MoS_2) to accelerate the catalytic conversion of LiPSs due to the improved conductivity from the 2H MoS_2 to metallic 1T phase transition and the introduction of sulfur vacancies (Fig. 7d). DFT studies demonstrated lower formation and decomposition energies for Li_2S on Co-MoS_2 than MoS_2. The enhanced catalytic property for Co-MoS_2 was revealed by the improved electrochemical performance in LSBs. Selecting suitable dopant with optimal LiPSs absorption is very important for high catalytic activity.[98] For nonmetallic atom doping, the electronegative P has been widely utilized. For example, P-doping was reported to activate the catalysis ability of MoS_2 basal planes.[96] P-doped MoS_2 exhibited strong Li-P and Mo-S bonds to immobilize soluble LiPSs and promoted cleavage of S-S or Li-S bonds to facilitate the LiPS redox kinetics. In addition to single element doping, multielement doping has also been proposed to boost the catalytic efficiency. Lin *et al*.[59] studied the simultaneous Co and P doping MoS_2 nanotubes (denoted as P-$Mo_{0.9}Co_{0.1}S_2$-2). Co-doping induced the 2H to the metallic 1T, whereas, the P doping introduced Co-P coordinated sites on the surface of

MoS_2 substrate, which could strongly promote the conversion between S and Li_2S. Finally, the Co-P coped MoS_2 enabled a stable sulfur cathode with a capacity of 886 mAh g^{-1} after 600 cycles at 1 C.

Introducing vacancies is another strategy for activating the catalyst surfaces.[99] The surface deficiencies can be either anion vacancies (*i.e.*, oxygen, sulfur) or cation vacancies (*i.e.*, Ti, Co). Li *et al.*[100] produced oxygen vacancies in TiO_2 (OVs-TiO_2) through the hydrogen annealing process. DFT calculations suggested that OVs could improve the absorptivity to LiPSs, catalytic ability, and ion/electron conductivity for TiO_2 catalysts. Different from the fast capacity degradation of LSBs with original TiO_2, OVs-TiO_2 modified LSBs stably operated for more than 100 cycles with a high capacity retention of 821 mAh^{-1} at a high m_{sl} of 7.1 mg cm^{-2}. Similarly, MoS_{2-x} nanoflakes,[56] $MoSe_{2-x}$,[24] and CoP_{1-x}[101] have also been synthesized and applied in cathode hosts or separators for high-sulfur-loading and lean-electrolyte LSBs.[24] In terms of cation-vacant catalysts, a case study was reported for Co-vacant-rich $ZnCo_{2-x}O_4$ as synthesized by partially replacing Co with Zn and in-situ etching of the Co_3O_4 template.[102] The Co defects significantly improved the anchoring and catalytic effects of the bimetallic oxide sheets. As a result, LSBs with an ultrahigh loading of 21.06 mg cm^{-2} and an areal capacity of 13.95 mAh cm^{-2} were achievable.

Above doping and vacancy defects can be simultaneously introduced to one catalyst system.[103, 104] Yao *et al.*[104] reported a P-doped and Te-vacant $NiTe_2$ nanoparticles (designed as P⊂$NiTe_{2-x}$). DFT calculations demonstrated the largest binding energies with sulfur species (Fig. 7e) and the lowest energy barriers for Li_2S oxidation and deposition for P⊂$NiTe_{2-x}$, in comparison with $NiTe_2$ and $NiTe_{2-x}$. Origins of the outstanding properties for P⊂$NiTe_{2-x}$ are the enhanced conductivity and chemical adsorption of LiPSs from Te-vacancies and the electronic structure change of Te from P doping. When loading P⊂$NiTe_{2-x}$-maize-straw carbon nanosheets on separators (Fig. 7f), the advanced LSBs could achieved a high capacity of 7.37 mA cm^{-2} after 120 cycles under high sulfur loading (m_{sl} = 10.2 mg cm^{-2}) and lean electrolyte (E/S ratio = 3.9 μL mg^{-1}) conditions.

4.3 Quantum dot catalysts

Apart from atomic-level design, nanostructure engineering can also realize appreciable catalytic efficiency by fully exposing the catalytically active sites or facets. Downsizing bulk catalytic materials into ultrafine-quantum

dots (QD) is an attractive direction to reshape the catalytic behaviors by unique quantum confinement and edge effects. So far, numerous QDs have been successfully prepared and applied in LSBs, such as black phosphorus QDs (BPQDs),[52] carbon nitride QDs (C_2N, C_4N),[105, 106] and carbon QDs.[107] 2D materials with unequal catalysis properties on edge and terrace areas are the most commonly used starting materials for QDs preparation. For example, the LiPS absorption and catalysis capabilities of the BP edges are higher than the basal planes.[52, 105] To maximize the catalyst efficiency of BP, our group sonicated large BP flakes to BPQDS as the catalyst in porous CNF/S cathodes.[52] The battery test illustrated the superiority of BPQD-mediated sulfur cathodes with remarkable capacity retentions of 95% (~800 mAh g^{-1}), 90%(~680 mAh g^{-1}, and 89% (~520 mAh g^{-1}) under high mass loadings of 4 mg cm^{-2}, 6 mg cm^{-2}, 8 mg cm^{-2}, respectively. QD synthesis can not only magnify the active sites but also induce prevailing phases for 2D materials.[53] For example, Yu *et al*.[108] found that 1T'-$MoTe_2$ QD derived from the 2H phase exhibited better chemisorption and catalysis properties. 1T'-$MoTe_2$ also displayed much higher electrical conductivity and chemical stability. In presence of the 3 nm-sized 1T'-$MoTe_2$ catalyst (Fig. 8a), the Li-S pouch cell demonstrated a reversible capacity of 658.7 mAh g^{-1} and 70.9% capacity retention at low E/S ratio of 5.5 μL mg^{-1} (Fig. 8b).

Water-soluble QDs with excellent thermal and chemical stability have also been synthesized for practical LSBs. Hu *et al*.[52, 105] reported 5 nm-sized C_2NQDs via a top-down approach to modify the separator in high-loading LSBs. Different from the bulk counterpart, C_2NQDs are more favorable for trapping and catalyzing the LiPS conversion arising from the synergy between the enriched active edge sites and the abundant oxygenated functional groups. A simulation study showed that the edge oxygen-carrying groups could lower the Li_2S decomposition energy barrier from 1.12 eV (at the terrace) to 0.65 eV. As a result, Li-S cells using C_2NQDs modified separators produced a large areal capacity (7.0 mAh cm^{-2}) at a high sulfur loading of 8.0 mg cm^{-2}.

Functional nanodots (NDs) have also been reported to modify cathode hosts and separators. The surface of MXene with abundant polar groups (*i.e.*, -OH, O, and F) possesses strong absorptions to LiPSs. Therefore, Xiao *et al*.[54] prepared MXene NDs to amplify the surface terminations (Fig. 8c). The carbon-free sulfur cathode using MXene ND/nanosheet host achieved high areal/volumetric capacities of 13.7 mAh cm^{-2}/1957 mAh cm^{-3} at a high m_{sl} of

13.8 mg cm^{-2} and moderate E/S ratio of 10 μL mg^{-1} (Fig. 8d). Apart from 2D materials, NDs of discrete molecular inorganic metal-oxide clusters with reversible multi-electron redox capability have also been explored. For example, Ni *et al*.[109] prepared a sulfur cathode with Keggin-type $H_3PW_{12}O_{40}$ (PW_{12}) NDs decorated on 3D rGO-CNT skeleton (rGO-CNT/PW_{12}@S). The 3D rGO-CNT structure provides a conductive network to accommodate the low conductivities of PW_{12}@S. The PW_{12} could positively catalyze the LiPS reaction and lithium sulfides oxidation during discharge/charge cycles. In particular, PW_{12} was transferred to HPB ($[PW_{12}O_{40}]_{7-}$) to catalyze Li_2S dissolution and returned back to PW_{12} during LiPS reduction. Owing to the bidirectional catalysis, the Li-S pouch cell with rGO-CNT/PW_{12}@S cathodes attained over 90% capacity retentions after 140 cycles at high sulfur loadings of 4 and 6.5 mg cm^{-2}.

4.4 Heterostructure catalysts

As mentioned in *Section 3.3*, the complexity of the Li-S chemistry makes it infeasible for a single catalyst to regulate all the conversion steps without sacrificing the properties of strong adsorption to LiPS and high electronic conductivity. Combining different catalysts with complementary functionalities into heterostructure is regarded as promising to potentially achieve "1+1>2" synergistic effects. The heterostructure interface with tremendous defects exhibits exceptionally high catalytic efficiency and smooth LiPS "trapping-discussion-conversion" pathways.[62] In this section, we will survey on the emerging heterostructure catalysts in practical LSBs.

2D heterostructure possessing ultrahigh surface-to-volume ratios has been intensively studied.[110] For example, pristine MoS_2 is a semiconductor with fair LiPS affinity at the basal plane. To remedy these weaknesses, metallic MoN was combined with MoS_2 nanosheet to form a MoS_2-MoN heterostructure.[75] The MoS_2 played the role to provide Li^+ diffusion routes, while MoN was responsible to improve the redox reaction process. Besides, MoN would participate in the Li_2S_6 and Li_2S_4 conversion reaction ($2Li_2S_6 + 3Li + Mo_3^+ \rightarrow 3Li_2S_4 + Mo_6^+$) to offer coupled electrons. Owning to the synergy of MoS_2 and MoN (Fig. 9a), the MoS_2/MoN-based LSBs exhibited an area capacity of 5.2 mAh cm^{-2} after 200 cycles at a remarkably high m_{sl} of 12.2 mg cm^{-2} and low E/S ratio of 6.3 μL mg^{-1} (Fig. 9b). Following this direction, many 2D heterostructures have been explored, such as WS_2-WO_3,[111] ZnS-SnS [112], SnS_2-SnO_2 [113] and MoN-VN [114].

Dispersing 0D nanoparticles on 2D sheets is another promising method to build multifunctional heterostructures. For example, Ye *et al.*[115] decorated CoZn-Se nanoparticles on nitrogen-doped MXene (N-MX) for sulfur cathodes (S/CoZn-Se@N-MX). The MXene skeleton provided fast electron/ion transport pathways and large surface area for CoZn-Se dispersion. The CoZn-Se could improve the sulfur reaction kinetics and prevent restacking of N-MX nanosheets (Fig. 9c). Li-S cells using S/CoZn-Se@N-MX cathodes with high m_{sl} = 7.8 mg cm^{-2} and low E/S ratio = 5 μL mg^{-1} achieved an areal capacity of 6.6 mAh cm^{-2} over 30 cycles (Fig. 9d). Similarly, other intriguing 0D-2D heterostructure catalysts have been reported for advanced LSBs, such as TiO_2-MXene[64], CoS_2-MXene[116], SnS_2/graphene[117].

3D heterostructure with large empty space for sulfur loading and facilitated electrolyte percolation has also been constructed. For example, ZnS-SnS nanobox was coated with a polydopamine-derived N-doped carbon to modify the separator in LSBs.[112] The ZnS-SnS heterojunction combined the functionalities of SnS (strong chemical binding to LiPSs and high conductivity) and ZnS (great catalytic ability). The ZnS-SnS@NC heterostructure was demonstrated effective to suppress the LiPS shuttle effect and uniform the Li metal deposition (Fig. 9e). The heterointerfaces between twinborn ZnS and SnS were clearly observed by HRTEMs (Fig. 9f). They were believed to boost the conversion kinetics, absorption to LiPS, and rapid diffusion of Li-ion. The cell using ZnS-SnS@NC modified separator achieved areal capacities of 9.46 mAh cm^{-2} for the first 15 cycles and remained at 8.27 mAh cm^{-2} after 100 cycles under harsh conditions of m_{sl} = 10.3 mg cm^{-2} and E/S ratio = 4 μl mg^{-1} (Fig. 9g).

4.5 Other emerging catalysts

In addition to above nanostructure engineering strategies for effective catalysts, new materials have also been explored in LSBs like metal phosphides [9, 118], metal borides [119, 120] and metal selenides [24, 121], and organic electrocatalysts[122, 123]. Here we only introduce emerging metal-based catalysts.

Transition-metal phosphides have excellent conductivity, however, pure metal phosphides with a reduced surface can hardly immobilize soluble LiPSs. The oxidation layers on the surface of metal phosphides activate the metal absorption to LiPSs, which has been confirmed in CoP, Ni_2P, FeP, MoP.[118] Zhou *et al.*[9] compared Co-based compounds (Co_3O_4, CoS_2, Co_4N, and CoP) to explore the anion influence. Among these Co-based compounds,

the S@rGO/CoP cathode showed the smallest overpotential, highest specific capacity (Fig. 10a) and best rate performance (Fig. 10b). The specific capacity of the cell can achieve 4.7 mAh cm^{-2} with a m_{sl}=5.2 mg cm^{-2} and E/S ratio= 10 µl mg^{-1} at 0.5C. The great electrochemical performance is attributed to the suitable adsorption ability and great diffusion dynamics, which are brought from P anion. The relationship between the energy gap (*p* and *d* band center) and overpotential of different Co-based compounds is demonstrated in Fig. 10c to illustrate the anion influence.

Metal boride materials own unique electronic structure, an empty 2*p* orbital, which attributes a strong trapping ability to LiPSs. Besides, their metallic character brings a high electrical conductivity.[124] CoB possesses 'synergistic adsorption' to soluble LiPSs for both Co and B can bind with S_4^{2-}, which is different from most of the metal components only display a single metal−sulfur absorption site (Fig. 10d).[119] The CoB also facilitated the Li_2S_8 nucleation and deposition. Therefore, the cell with CoB/CNT modified separator attained an areal capacity of 5.5 mAh cm^2 at 0.5 C with a m_{sl}= 5.8 mg cm^{-2} (Fig. 10e). He *et al*. [120] reported MoB/S cathode with a m_{sl}=6.1 mg cm^{-2} and E/S ratio = 7µl mg^{-1} demonstrates an high initial capacity of 780 mA h g^{-1}(4.75 mA h cm^{-2}) and remain 83% capacity after 200 circles at 0.2C. This superior performance is attributed to the good conductivity, abundance of active sites, nanosized morphology, and good wettability to electrolytes of MoB. Metal selenide attracts much attention due to the great catalytic effect and better conductivity than metal sulfides. Yuan *et al*.[125] reported using $CoSe_2$ nanodots on graphene build electrolyte/$CoSe_2$/G triple-phase interface. The $CoSe_2$ played the roles to absorb the soluble LiPSs and improve the sulfur species conversion kinetics. The cell performs a high specific capacity of 1098 mAh g^{-1} with a m_{sl}=4.35 mg cm^{-2} and E/S ratio of 15 µl mg^{-1} at 0.2C. Co_3Se_4 with high conductive and catalytic has been introduced 3D N-doped carbon matrix; the host shows great ability to immobilize LiPSs and catalyze the sulfur species reversion kinetics as shown in Fig. 10f [126]. Therefore, even with m_{sl}=3.1 mg cm^{-2}, the cell can stably work more than 800 cycles with a low capacity decay rate of 0.067%.

Ensuring LSBs stable operation in high sulfur loading and low E/S ratio environment is an important condition to achieve practical cell. Catalysts are regarded as a potential solution to architect practical LSBs. According to

give insight into the emerging catalysts, it is favorable to understand the requirements to develop emerging catalysts. Exploring novel materials is not the only method to explore the emerging catalysts, take the design principles into consideration to improve the catalyst efficiency are major direction to optimal the catalysts. For instance, the quantum dot and single atoms through decreasing size can provide more exposure to active sites, decreasing catalysts loading. Heterostructure can combine the advantages of different materials as well as introduce novel interfaces with high catalytic ability. Defect engineering improves the intrinsic activity and conductivity of catalyst. Therefore, to achieve high energy density Li-S cells, the design of emerging catalysts should satisfy the requirements of great conductivity, high catalytic efficiency, suitable trapping ability to LiPSs, and low weight percentages in the system.

5. Statistical analysis the electrochemical performance of Li-S batteries with catalysts

In order to give an insight into the performance advancement of the emerging catalysts modified LSBs under high-sulfur-loading and lean-electrolyte conditions, we statistically analyzed the electrochemical performance of 90 representative papers published in the last 5 years (2018-2022)[11, 52-54, 58, 64, 66, 69, 74-76, 84, 105, 106, 108, 111, 112, 114-116, 120, 125-193]. The key parameters in terms of the specific capacity (in idea condition: flooded electrolyte and low sulfur loading, practical condition: high sulfur loading and lean electrolyte), sulfur loading, sulfur content (based on the weight cathode), areal capacity (based on the initial specific capacity), cycle life (based on the high sulfur loading cycling) and catalyst content (based on the cathode) are summarized in Figs. 11 and 12.

For the initial cyclic performance, it shows that approximately 90% of catalyst-modified cells present specific capacities beyond 1000 mAh g^{-1} (referring to 60% sulfur utilization) in ideal conditions (Fig. 11a). However, this percentage sharply decreased to 34% under lean-electrolyte (E/S ratio <10 uL mg^{-1}) and/or high-sulfur-loading (m_{sl} >4 mg cm^{-2}) conditions (Fig. 11b). Regarding the areal capacity (equal to specific capacity × areal sulfur loading), almost 90% of the cells presented capacities greater than 3 mAh cm^{-2}, but only a fifth surpassed 7 mAh cm^{-2} (Fig. 11c). We need to explain that 7 mAh cm^{-2} is an important standard for LSBs to compete with state-of-the-art LIBs, given the fact that LSBs have an operating voltage of 2.1 V, which is lower than the 3.5V for

commercial LIBs with areal capacities over 4 mAh cm^{-2}. Fig. 11 indicates that the sulfur utilization has been significantly improved by emerging catalysts but there is still a large discrepancy between the performance tested under ideal and practical conditions.

The key parameters suggested in *Section 2* for building high-energy-density LSBs (for example 400 to 500 Wh kg^{-1}) are m_{sl} of >8 mg cm^{-2}, the sulfur content of >70wt%, E/S ratio of <3 μL mg^{-1}, and sulfur utilization of >70%. The chart maps in Figs. 12a-c show that a quarter of the cells have sulfur content of >70%, around 41% of electrodes exhibit sulfur loadings above 8 mg cm^{-2} but only 4.7% limited the E/S below 5 μL mg^{-1}. Clearly, validated progress has been obtained for high loading and high content sulfur cathodes but it is still of a profound challenge to approach low E/S, potentially due to the large surface area and high porosity of nanomaterial cathodes requiring considerable amounts of electrolyte for cell wetting. In terms of cyclic stability, over half of the high-loading cells exhibited lifetimes of 100-300 cycles, and several up to 600 cycles (Fig. 12d). In terms of the catalyst content, 11% of cells reported catalyst contents of <2 wt%, nevertheless, over half of the cells contained catalysts of >10 wt% (Fig. 12e). Thus, how to further decrease the catalyst content and improve the catalytic efficiency requires more effort.

When we compared the above data with those summarized between 2018-2022,[17, 194, 195] it clearly shows that awareness of the importance of the E/S ratio has been widely recognized with almost 100% of representative papers reporting this parameter, which is less than one quarter in the previous survey [194]. Other notable progresses are observed in the percentage increment of high sulfur loading (12.28 % vs 88% for m_{sl} >4 mg cm^{-2}), high areal capacities (19.23% vs 70.6% for C_{areal} >4 mAh cm^{-2}) and extended cycle life for high-loading electrodes. The above statistical comparisons suggest that catalysis is a promising solution for practical LSBs. Nerveless, there are still key problems remaining to be solved based on the above evaluations: (i) the specific capacities of the cells are far below the energy requirement under high loading and lean electrolyte conditions; (ii) mostly reported E/S ratios are still above 5 μL mg^{-1}; and (iii) the cycle life of Li-S pouch cells is only tens of cycles, far from sufficient to satisfy the requirement for practical LSBs.

6. Conclusion and perspective

LSBs with high energy density and high abundance of sulfur have shown great potential for the next-generation energy-storage system. In the past decade with an in-depth understanding and regulation of the Li-S chemistry, remarkable advances have been achieved in developing high-performance Li-S cells in the laboratory. To fulfill the original goal and promote practical LSB in the market, increasing attention are now paid to research on LSBs with high sulfur loading, low E/S ratio and limited anode excess. Such harsh restrictions redefine the challenges in LSBs research, including the sluggish reaction kinetics, low sulfur utilization and unstable lithium metal anode. To solve these issues and construct practical high-energy-density LSBs, the concept of the catalysis effect has been proposed effective. To avoid duplication with numerous reviews about catalysts in LSBs, this paper examined a series of emerging catalytic materials with different dimensions and functionalities. To effectively regulate the more complex Li-S chemistry in practical conditions, catalyst design principles are initially proposed, including abundant active sites, multifunctional capability and synergy of different components. On the base of a clear understanding of the emerging challenges and potential tools at hand, we then elaborate the state-of-the-art catalytic materials from the atomic level to the macro level and from single components to heterostructures. It is observed that the catalytic effect significantly accelerated the reaction kinetics, stabilize the Li metal anodes, and finally boost the electrochemical performance of LSBs under high-sulfur-loading and lean-electrolyte conditions. Despite the considerable progress that has been made over the past years, several challenges related to the strong discrepancy between high-level academic achievements but limited battery performance at the prototype cell level are still observed via statistical analysis of the data from 90 representative papers. To further enhance the catalytic efficiency to build practical LSBs, some key points are suggested for the further development of catalytic materials.

(1) Rationalize the weight ratio of catalysts.

Catalysts are functional to realize uniform adsorption of LiPSs and deposition/dissolution of the Li_2S in cathodes, redistribute the Li-ion flux for dendrite-free Li metal deposition in anodes, and to mediate the chemical reactions in electrolytes. However, catalytic materials are electrochemically inert, which means too many catalysts discourage the high-energy merit of LSBs but too little leads to insufficient catalytic effects. Therefore, apart from

boosting the catalytic efficiency of emerging materials, it is also important to strike a balance between cyclic stability and the energy density of LSBs regulated by effective catalysts.

(2) In-depth understanding of the catalytic mechanisms

The current research focuses on the exploration of novel catalytic materials in LSBs, while understandings of the detailed catalytic and degradation mechanisms have yet to receive much attention. It was taken as a grant that the battery performance degradation is related to sulfur electrode instability without considering the deterioration of the catalysis and adsorption capability of catalysts. Indeed, chemical/electrochemical reactions between LiPSs/Li salts and catalysts happen, possibly leading to catalyst poisoning during cycles, for example, a surface gel layer will generate on the MoS_2 surface due to the interaction between LiTFSI and MoS_2.[196, 197]. In addition, advanced characterizations, especially in-situ observations, enabling instantaneous detection of the Li-S reactions and catalysis process are still lacking. These techniques can assist to establish the fundamental theory to guide the design and fabrication of powerful catalytic materials.

(3) Establish a standard to evaluate the catalytic efficiency

When we statistically analyze the electrochemical performance of Li-S cells using catalysts, it is found that a direct comparison of the catalytic efficiency is not trivial. On one hand, the information on catalyst content/loading is missing for fundamental studies, making it infeasible to conduct peer comparisons. On the other hand, Li-S cells with catalyst materials are measured in significantly different protocols and cell parameters, impeding the effort to directly rank their performance as in commercial LIBs. Therefore, it is suggested that standard protocols and cell parameters should be proposed and followed by the community in future studies of catalytic materials in practical LSBs. In addition to the above fundamental concerns, the manufacturing cost, the cell configurations and the environmental safety should also be taken into account as they determine whether the catalyst-containing LSBs can compete with current rechargeable battery technologies.

Conflicts of interest

There are no conflicts to declare.

Acknowledgements

This work described in this paper was fully supported by grants from the Research Grants Council of the Hong Kong Special Administrative Region, China (Project No. PolyU25216121, PolyU15303219), the National Natural Science Foundation of China for Young Scholar (Project No. 52102310), the Research Committee of the Hong Kong Polytechnic University under project codes of A-PB1M, 1-BBXK, 1-CD4M, and G-UAMV.

Notes and references

[1] G. Zhou, H. Chen, Y. Cui, Nat. Energy, 7 (2022) 312-319.

[2] J. Li, C. Ren, L. Zhang, W. Jiang, H. Liu, J. Su, M. Li, J. Energy Chem., 65 (2022) 205-209.

[3] Y.Q. Peng, M. Zhao, Z.X. Chen, Q. Cheng, Y. Liu, C.X. Zhao, X. Ma, B.Q. Li, C.M. Chen, J.Q. Huang, Q. Zhang, Batteries & Supercaps, 5 (2021) e202100359.

[4] S.H. Chung, C.H. Chang, A. Manthiram, Adv. Funct. Mater., 28 (2018) 1801188.

[5] F. Shi, C. Chen, Z.-L. Xu, Advanced Fiber Materials, 3 (2021) 275-301.

[6] X. Ji, K.T. Lee, L.F. Nazar, Nat. Mater., 8 (2009) 500-506.

[7] X. Chen, H. Ji, Z. Rao, L. Yuan, Y. Shen, H. Xu, Z. Li, Y. Huang, Adv. Energy Mater., 12 (2021) 2102774.

[8] Y. Ding, Q. Cheng, J. Wu, T. Yan, Z. Shi, M. Wang, D. Yang, P. Wang, L. Zhang, J. Sun, Adv. Mater., (2022) e2202256.

[9] J. Zhou, X. Liu, L. Zhu, J. Zhou, Y. Guan, L. Chen, S. Niu, J. Cai, D. Sun, Y. Zhu, J. Du, G. Wang, Y. Qian, Joule, 2 (2018) 2681-2693.

[10] Z. Xiao, Z. Yang, L. Zhang, H. Pan, R. Wang, ACS Nano, 11 (2017) 8488-8498.

[11] H. Zhang, L.K. Ono, G. Tong, Y. Liu, Y. Qi, Nat. Commun., 12 (2021) 4738.

[12] R. Li, D. Rao, J. Zhou, G. Wu, G. Wang, Z. Zhu, X. Han, R. Sun, H. Li, C. Wang, W. Yan, X. Zheng, P. Cui, Y. Wu, G. Wang, X. Hong, Nat. Commun., 12 (2021) 3102.

[13] G. Ye, M. Zhao, L.-P. Hou, W.-J. Chen, X.-Q. Zhang, B.-Q. Li, J.-Q. Huang, Journal of Energy Chemistry, 66 (2022) 24-29.

[14] M. Zhao, B.Q. Li, X.Q. Zhang, J.Q. Huang, Q. Zhang, ACS Cent. Sci., 6 (2020) 1095-1104.

[15] C.X. Bi, M. Zhao, L.P. Hou, Z.X. Chen, X.Q. Zhang, B.Q. Li, H. Yuan, J.Q. Huang, Adv. Sci., 9 (2022) e2103910.

[16] T. Cleaver, P. Kovacik, M. Marinescu, T. Zhang, G. Offer, J. Electrochem. Soc., 165 (2017) A6029-A6033.

[17] X. Yang, X. Li, K. Adair, H. Zhang, X. Sun, Electrochemical Energy Reviews, 1 (2018) 239-293.

[18] Y. Chen, T. Wang, H. Tian, D. Su, Q. Zhang, G. Wang, Adv. Mater., 33 (2021) e2003666.

[19] Z.X. Chen, M. Zhao, L.P. Hou, X.Q. Zhang, B.Q. Li, J.Q. Huang, Adv. Mater., (2022) e2201555.

[20] S. Dörfler, H. Althues, P. Härtel, T. Abendroth, B. Schumm, S. Kaskel, Joule, 4 (2020) 539-554.

[21] M. Cheng, R. Yan, Z. Yang, X. Tao, T. Ma, S. Cao, F. Ran, S. Li, W. Yang, C. Cheng, Adv. Sci., 9 (2022) e2102217.

[22] P. Wang, F. Sun, S. Xiong, Z. Zhang, B. Duan, C. Zhang, J. Feng, B. Xi, Angew. Chem. Int. Ed., 61 (2022) e202116048.

[23] Y. Tsao, H. Gong, S. Chen, G. Chen, Y. Liu, T.Z. Gao, Y. Cui, Z. Bao, Adv. Energy Mater., 11 (2021) 2101449.

[24] M. Wang, Z. Sun, H. Ci, Z. Shi, L. Shen, C. Wei, Y. Ding, X. Yang, J. Sun, Angew. Chem. Int. Ed., 60 (2021) 24558-24565.

[25] W. Wang, L. Huai, S. Wu, J. Shan, J. Zhu, Z. Liu, L. Yue, Y. Li, ACS Nano, (2021) 11619−11633.

[26] H.-J. Peng, J.-Q. Huang, X.-B. Cheng, Q. Zhang, Adv. Energy Mater., 7 (2017) 1700260.

[27] M. Zhao, B.Q. Li, H.J. Peng, H. Yuan, J.Y. Wei, J.Q. Huang, Angew. Chem. Int. Ed., 59 (2020) 12636-12652.

[28] S.-H. Chung, A. Manthiram, Joule, 2 (2018) 710-724.

[29] J. Liu, Z. Bao, Y. Cui, E.J. Dufek, J.B. Goodenough, P. Khalifah, Q. Li, B.Y. Liaw, P. Liu, A. Manthiram, Y.S. Meng, V.R. Subramanian, M.F. Toney, V.V. Viswanathan, M.S. Whittingham, J. Xiao, W. Xu, J. Yang, X.-Q. Yang, J.-G. Zhang, Nat. Energy, 4 (2019) 180-186.

[30] A. Gupta, A. Bhargav, A. Manthiram, Adv. Energy Mater., 9 (2019) 1803096.

[31] Y. Hu, W. Chen, T. Lei, Y. Jiao, J. Huang, A. Hu, C. Gong, C. Yan, X. Wang, J. Xiong, Adv. Energy Mater., 10 (2020) 2000082.

[32] Y.-Q. Peng, M. Zhao, Z.-X. Chen, Q. Cheng, Y. Liu, X.-Y. Li, Y.-W. Song, B.-Q. Li, J.-Q. Huang, Nano Res., (2022).

[33] K.L. Gering, Electrochim. Acta, 51 (2006) 3125-3138.

[34] L. Wang, Y. Ye, N. Chen, Y. Huang, L. Li, F. Wu, R. Chen, Adv. Funct. Mater., 28 (2018) 1800919.

[35] J. Conder, R. Bouchet, S. Trabesinger, C. Marino, L. Gubler, C. Villevieille, Nat. Energy, 2 (2017) 17069.

[36] J. Guo, H. Pei, Y. Dou, S. Zhao, G. Shao, J. Liu, Adv. Funct. Mater., 31 (2021) 2010499.

[37] Y.-C. Chien, A.S. Menon, W.R. Brant, M.J. Lacey, D. Brandell, J. Phys. Chem. C, 126 (2022) 2971-2979.

[38] Z.W. Seh, Y. Sun, Q. Zhang, Y. Cui, Chem. Soc. Rev., 45 (2016) 5605-5634.

[39] L. Kong, Q. Jin, X.-T. Zhang, B.-Q. Li, J.-X. Chen, W.-C. Zhu, J.-Q. Huang, Q. Zhang, Journal of Energy Chemistry, 39 (2019) 17-22.

[40] X. Zhang, Y. Chen, F. Ma, X. Chen, B. Wang, Q. Wu, Z. Zhang, D. Liu, W. Zhang, J. He, Z.-L. Xu, Chem. Eng. J., 436 (2022) 134945.

[41] W.G. Lim, S. Kim, C. Jo, J. Lee, Angew. Chem. Int. Ed., 58 (2019) 18746-18757.

[42] W. Hua, H. Li, C. Pei, J. Xia, Y. Sun, C. Zhang, W. Lv, Y. Tao, Y. Jiao, B. Zhang, S.Z. Qiao, Y. Wan, Q.H. Yang, Adv. Mater., 33 (2021) e2101006.

[43] P. Zeng, C. Liu, X. Zhao, C. Yuan, Y. Chen, H. Lin, L. Zhang, ACS Nano, 14 (2020) 11558-11569.

[44] J. Guo, Y. Huang, S. Zhao, Z. Li, Z. Wang, G. Shao, J. Liu, ACS Nano, 15 (2021) 16322-16334.

[45] G. Li, X. Wang, M.H. Seo, M. Li, L. Ma, Y. Yuan, T. Wu, A. Yu, S. Wang, J. Lu, Z. Chen, Nat. Commun., 9 (2018) 705.

[46] J.L. Yang, D.Q. Cai, X.G. Hao, L. Huang, Q. Lin, X.T. Zeng, S.X. Zhao, W. Lv, ACS Nano, (2021) 11491−11500.

[47] P. Wang, B. Xi, M. Huang, W. Chen, J. Feng, S. Xiong, Adv. Energy Mater., 11 (2021) 2002893.

[48] Q. Shao, P. Lu, L. Xu, D. Guo, J. Gao, Z.-S. Wu, J. Chen, Journal of Energy Chemistry, 51 (2020) 262-271.

[49] M. Zhao, H.J. Peng, B.Q. Li, X. Chen, J. Xie, X. Liu, Q. Zhang, J.Q. Huang, Angew. Chem. Int. Ed., 59 (2020) 9011-9017.

[50] J. He, G.90 Hartmann, M. Lee, G.S. Hwang, Y. Chen, A. Manthiram, Energy Environ. Sci. , 12 (2019) 344-350.

[51] Z.W. Seh, J. Kibsgaard, C.F. Dickens, I. Chorkendorff, J.K. Norskov, T.F. Jaramillo, Science, 355 (2017) eaad4998.

[52] Z.L. Xu, S. Lin, N. Onofrio, L. Zhou, F. Shi, W. Lu, K. Kang, Q. Zhang, S.P. Lau, Nat. Commun., 9 (2018) 4164.

[53] Z.-L. Xu, N. Onofrio, J. Wang, J. Mater. Chem. A, 8 (2020) 17646-17656.

[54] Z. Xiao, Z. Li, P. Li, X. Meng, R. Wang, ACS Nano, 13 (2019) 3608-3617.

[55] H. Wang, Q. Zhang, H. Yao, Z. Liang, H.W. Lee, P.C. Hsu, G. Zheng, Y. Cui, Nano Lett., 14 (2014) 7138-7144.

[56] H. Lin, L. Yang, X. Jiang, G. Li, T. Zhang, Q. Yao, G.W. Zheng, J.Y. Lee, Energy Environ. Sci. , 10 (2017) 1476-1486.

[57] W. Zhou, L. Ma, D. Zhao, J. Li, Z. Chen, W. Mai, N. Wang, L. Li, Small, (2022) e2200405.

[58] Z. Shen, Z. Zhang, M. Li, Y. Yuan, Y. Zhao, S. Zhang, C. Zhong, J. Zhu, J. Lu, H. Zhang, ACS Nano, 14 (2020) 6673-6682.

[59] H. Lin, S. Zhang, T. Zhang, H. Ye, Q. Yao, G.W. Zheng, J.Y. Lee, Adv. Energy Mater., 9 (2019) 1902096.

[60] J. Huang, Y. Jiang, T. An, M. Cao, J. Mater. Chem. A, 8 (2020) 25465-25498.

[61] K. Mahankali, S.V. Gottumukkala, N. Masurkar, N.K. Thangavel, R. Jayan, A. Sawas, S. Nagarajan, M.M. Islam, L.M.R. Arava, ACS Appl. Mater. Interfaces, (2022) 24486–24496.

[62] T. Zhou, W. Lv, J. Li, G. Zhou, Y. Zhao, S. Fan, B. Liu, B. Li, F. Kang, Q.-H. Yang, Energy Environ. Sci. , 10 (2017) 1694-1703.

[63] R. Razaq, D. Sun, J. Wang, Y. Xin, G. Abbas, J. Zhang, Q. Li, T. Huang, Z. Zhang, Y. Huang, J. Power Sources, 414 (2019) 453-459.

[64] L. Jiao, C. Zhang, C. Geng, S. Wu, H. Li, W. Lv, Y. Tao, Z. Chen, G. Zhou, J. Li, G. Ling, Y. Wan, Q.H. Yang, Adv. Energy Mater., 9 (2019) 1900219.

[65] W. Hua, H. Li, C. Pei, J. Xia, Y. Sun, C. Zhang, W. Lv, Y. Tao, Y. Jiao, B. Zhang, S.Z. Qiao, Y. Wan, Q.H. Yang, Adv. Mater., 33 (2021) 2101006.

[66] L. Chen, Y. Xu, G. Cao, H.M.K. Sari, R. Duan, J. Wang, C. Xie, W. Li, X. Li, Adv. Funct. Mater., 32 (2021) 2107838.

[67] R. Wang, C. Luo, T. Wang, G. Zhou, Y. Deng, Y. He, Q. Zhang, F. Kang, W. Lv, Q.H. Yang, Adv. Mater., 32 (2020) e2000315.

[68] C. Yuan, X. Yang, P. Zeng, J. Mao, K. Dai, L. Zhang, X. Sun, Nano Energy, 84 (2021) 105928.

[69] X.J. Hong, C.L. Song, Y. Yang, H.C. Tan, G.H. Li, Y.P. Cai, H. Wang, ACS Nano, 13 (2019) 1923-1931.

[70] H. Ci, M. Wang, Z. Sun, C. Wei, J. Cai, C. Lu, G. Cui, Z. Liu, J. Sun, J. Energy Chem., 66 (2022) 474-482.

[71] Y. Li, S. Lin, D. Wang, T. Gao, J. Song, P. Zhou, Z. Xu, Z. Yang, N. Xiao, S. Guo, Adv. Mater., 32 (2020) e1906722.

[72] Z.-L. Xu, S.J. Kim, D. Chang, K.-Y. Park, K.S. Dae, K.P. Dao, J.M. Yuk, K. Kang, Energy Environ. Sci., 12 (2019) 3144-3155.

[73] L. Hu, C. Dai, H. Liu, Y. Li, B. Shen, Y. Chen, S.-J. Bao, M. Xu, Adv. Energy Mater., 8 (2018) 1800709.

[74] M. Wang, Y. Song, Z. Sun, Y. Shao, C. Wei, Z. Xia, Z. Tian, Z. Liu, J. Sun, ACS Nano, 13 (2019) 13235-13243.

[75] S. Wang, S. Feng, J. Liang, Q. Su, F. Zhao, H. Song, M. Zheng, Q. Sun, Z. Song, X. Jia, J. Yang, Y. Li, J. Liao, R. Li, X. Sun, Adv. Energy Mater., 11 (2021) 2003314.

[76] C. Zhao, G.L. Xu, Z. Yu, L. Zhang, I. Hwang, Y.X. Mo, Y. Ren, L. Cheng, C.J. Sun, Y. Ren, X. Zuo, J.T. Li, S.G. Sun, K. Amine, T. Zhao, Nat. Nanotechnol., 16 (2021) 166-173.

[77] Z. Han, S. Zhao, J. Xiao, X. Zhong, J. Sheng, W. Lv, Q. Zhang, G. Zhou, H.M. Cheng, Adv. Mater., 33 (2021) e2105947.

[78] G. Zhou, H. Tian, Y. Jin, X. Tao, B. Liu, R. Zhang, Z.W. Seh, D. Zhuo, Y. Liu, J. Sun, J. Zhao, C. Zu, D.S. Wu, Q. Zhang, Y. Cui, Proc. Natl. Acad. Sci. U.S.A., 114 (2017) 840-845.

[79] G. Zhou, S. Zhao, T. Wang, S.Z. Yang, B. Johannessen, H. Chen, C. Liu, Y. Ye, Y. Wu, Y. Peng, C. Liu, S.P. Jiang, Q. Zhang, Y. Cui, Nano Lett., 20 (2020) 1252-1261.

[80] D. Wang, F. Li, R. Lian, J. Xu, D. Kan, Y. Liu, G. Chen, Y. Gogotsi, Y. Wei, ACS Nano, 13 (2019) 11078-11086.

[81] L. Fang, Z. Feng, L. Cheng, R.E. Winans, T. Li, Small Methods, 4 (2020) 2000315.

[82] C. Xia, Y. Qiu, Y. Xia, P. Zhu, G. King, X. Zhang, Z. Wu, J.Y.T. Kim, D.A. Cullen, D. Zheng, P. Li, M. Shakouri, E. Heredia, P. Cui, H.N. Alshareef, Y. Hu, H. Wang, Nat. Chem., 13 (2021) 887-894.

[83] S. Ji, Y. Chen, X. Wang, Z. Zhang, D. Wang, Y. Li, Chem. Rev., 120 (2020) 11900-11955.

[84] Z. Du, X. Chen, W. Hu, C. Chuang, S. Xie, A. Hu, W. Yan, X. Kong, X. Wu, H. Ji, L.J. Wan, J. Am. Chem. Soc., 141 (2019) 3977-3985.

[85] L. Zhang, D. Liu, Z. Muhammad, F. Wan, W. Xie, Y. Wang, L. Song, Z. Niu, J. Chen, Adv. Mater., 31 (2019) e1903955.

[86] C. Lu, Y. Chen, Y. Yang, X. Chen, Nano Lett., 20 (2020) 5522-5530.

[87] P. Zhai, T. Wang, W. Yang, S. Cui, P. Zhang, A. Nie, Q. Zhang, Y. Gong, Advanced Energy Materials, 9 (2019) 1804019.

[88] C.L. Song, Z.H. Li, L.Y. Ma, M.Z. Li, S. Huang, X.J. Hong, Y.P. Cai, Y.Q. Lan, ACS Nano, (2021) 13436−13443.

[89] H. Liu, X. Chen, X.B. Cheng, B.Q. Li, R. Zhang, B. Wang, X. Chen, Q. Zhang, Small Methods, 3 (2018) 1800354.

[90] Y. Sun, J. Zhou, H. Ji, J. Liu, T. Qian, C. Yan, ACS Appl. Mater. Interfaces, 11 (2019) 32008-32014.

[91] J. Gu, Q. Zhu, Y. Shi, H. Chen, D. Zhang, Z. Du, S. Yang, ACS Nano, 14 (2020) 891-898.

[92] K. Yan, Z. Lu, H.-W. Lee, F. Xiong, P.-C. Hsu, Y. Li, J. Zhao, S. Chu, Y. Cui, Nat. Energy, 1 (2016) 16010.

[93] T. Feng, T. Zhao, N. Zhang, Y. Duan, L. Li, F. Wu, R. Chen, Adv. Funct. Mater., (2022) 2202766.

[94] W. Liu, C. Luo, S. Zhang, B. Zhang, J. Ma, X. Wang, W. Liu, Z. Li, Q.H. Yang, W. Lv, ACS Nano, 15 (2021) 7491-7499.

[95] R. Zhang, Y. Dong, M.A. Al-Tahan, Y. Zhang, R. Wei, Y. Ma, C. Yang, J. Zhang, Journal of Energy Chemistry, 60 (2021) 85-94.

[96] F. Liu, N. Wang, C. Shi, J. Sha, L. Ma, E. Liu, N. Zhao, Chem. Eng. J. , 431 (2022) 133923.

[97] Y. Feng, H. Liu, Y. Liu, F. Zhao, J. Li, X. He, Journal of Energy Chemistry, 62 (2021) 508-515.

[98] Z. Shen, X. Jin, J. Tian, M. Li, Y. Yuan, S. Zhang, S. Fang, X. Fan, W. Xu, H. Lu, J. Lu, H. Zhang, Nat. Catal., 5 (2022) 555-563.

[99] M. Zhang, W. Chen, L. Xue, Y. Jiao, T. Lei, J. Chu, J. Huang, C. Gong, C. Yan, Y. Yan, Y. Hu, X. Wang, J. Xiong, Adv. Funct. Mater., 10 (2019) 1903008.

[100] Z. Li, C. Zhou, J. Hua, X. Hong, C. Sun, H.W. Li, X. Xu, L. Mai, Adv. Mater., 32 (2020) e1907444.

[101] R. Sun, Y. Bai, Z. Bai, L. Peng, M. Luo, M. Qu, Y. Gao, Z. Wang, W. Sun, K. Sun, Adv. Energy Mater., 12 (2022) 1904010.

[102] Z. Li, Q. Zhang, L. Hencz, J. Liu, P. Kaghazchi, J. Han, L. Wang, S. Zhang, Nano Energy, 89 (2021) 106331.

[103] Z. Shi, Z. Sun, J. Cai, X. Yang, C. Wei, M. Wang, Y. Ding, J. Sun, Adv. Mater., 33 (2021) e2103050.

[104] W. Yao, C. Tian, C. Yang, J. Xu, Y. Meng, I. Manke, N. Chen, Z. Wu, L. Zhan, Y. Wang, R. Chen, Adv. Mater., 34 (2022) e2106370.

[105] X. Hu, L. Zhong, C. Shu, Z. Fang, M. Yang, J. Li, D. Yu, J. Am. Chem. Soc., 142 (2020) 4621-4630.

[106] C. Shu, L. Fang, M. Yang, L. Zhong, X. Chen, D. Yu, Angew. Chem. Int. Ed., 61 (2022) e202114182.

[107] Y. Hu, W. Chen, T. Lei, B. Zhou, Y. Jiao, Y. Yan, X. Du, J. Huang, C. Wu, X. Wang, Y. Wang, B. Chen, J. Xu, C. Wang, J. Xiong, Adv. Energy Mater., 9 (2019) 1802955.

[108] B. Yu, A. Huang, K. Srinivas, X. Zhang, F. Ma, X. Wang, D. Chen, B. Wang, W. Zhang, Z. Wang, J. He, Y. Chen, ACS Nano, (2021) 3279−13288.

[109] L. Ni, G. Yang, Y. Liu, Z. Wu, Z. Ma, C. Shen, Z. Lv, Q. Wang, X. Gong, J. Xie, G. Diao, Y. Wei, ACS Nano, (2021) 12222−12236.

[110] J. Mei, T. Liao, Z. Sun, Energy Environ. Sci. , 5 (2021) 115-132.

[111] B. Zhang, C. Luo, Y. Deng, Z. Huang, G. Zhou, W. Lv, Y.B. He, Y. Wan, F. Kang, Q.H. Yang, Adv. Energy Mater., 10 (2020) 2000091.

[112] W. Yao, W. Zheng, J. Xu, C. Tian, K. Han, W. Sun, S. Xiao, ACS Nano, 15 (2021) 7114-7130.

[113] M. Wang, L. Fan, X. Wu, Y. Qiu, Y. Wang, N. Zhang, K. Sun, Chem. Eur. J. , 25 (2019) 5416-5421.

[114] C. Ye, Y. Jiao, H. Jin, A.D. Slattery, K. Davey, H. Wang, S.Z.J.A.C.I.E. Qiao, Angew. Chem. Int. Ed. , 57 (2018) 16703-16707.

[115] Z. Ye, Y. Jiang, L. Li, F. Wu, R. Chen, Adv. Mater., 33 (2021) e2101204.

[116] C. Yang, Y. Li, W. Peng, F. Zhang, X. Fan, Chem. Eng. J. , 427 (2022) 131792.

[117] D. Gao, Y. Wang, Y. Liu, H. Sun, M. Wu, H. Zhang, J. Colloid Interface Sci., 538 (2019) 116-124.

[118] Y. Zhong, L. Yin, P. He, W. Liu, Z. Wu, H. Wang, J. Am. Chem. Soc., 140 (2018) 1455-1459.

[119] B. Guan, Y. Zhang, L. Fan, X. Wu, M. Wang, Y. Qiu, N. Zhang, K. Sun, ACS Nano, 13 (2019) 6742-6750.

[120] J. He, A. Bhargav, A. Manthiram, Adv. Mater., 32 (2020) 2004741.

[121] B. Yuan, D. Hua, X. Gu, Y. Shen, L.-C. Xu, X. Li, B. Zheng, J. Wu, W. Zhang, S. Li, F. Huo, Journal of Energy Chemistry, 48 (2020) 128-135.

[122] C.X. Zhao, X.Y. Li, M. Zhao, Z.X. Chen, Y.W. Song, W.J. Chen, J.N. Liu, B. Wang, X.Q. Zhang, C.M. Chen, B.Q. Li, J.Q. Huang, Q. Zhang, J. Am. Chem. Soc., 143 (2021) 19865-19872.

[123] Y.-W. Song, J.-L. Qin, C.-X. Zhao, M. Zhao, L.-P. Hou, Y.-Q. Peng, H.-J. Peng, B.-Q. Li, J. Energy Chem., 64 (2022) 568-573.

[124] J. Li, Z. Niu, C. Guo, M. Li, W. Bao, Journal of Energy Chemistry, 54 (2021) 434-451.

[125] H. Yuan, H.-J. Peng, B.-Q. Li, J. Xie, L. Kong, M. Zhao, X. Chen, J.-Q. Huang, Q. Zhang, Adv. Energy Mater., 9 (2019) 1802768.

[126] D. Cai, B. Liu, D. Zhu, D. Chen, M. Lu, J. Cao, Y. Wang, W. Huang, Y. Shao, H. Tu, W. Han, Adv. Energy Mater., 10 (2020) 1904273.

[127] Z. Wang, K. Yu, Y. Feng, R. Qi, J. Ren, Z. Zhu, ACS Appl. Mater. Interfaces, 11 (2019) 44282-44292.

[128] K. Zhang, Z. Chen, R. Ning, S. Xi, W. Tang, Y. Du, C. Liu, Z. Ren, X. Chi, M. Bai, C. Shen, X. Li, X. Wang, X. Zhao, K. Leng, S.J. Pennycook, H. Li, H. Xu, K.P. Loh, K. Xie, ACS Appl. Mater. Interfaces, 11 (2019) 25147-25154.

[129] Y. Chen, W. Zhang, D. Zhou, H. Tian, D. Su, C. Wang, D. Stockdale, F. Kang, B. Li, G. Wang, ACS Nano, 13 (2019) 4731-4741.

[130] H. Ci, J. Cai, H. Ma, Z. Shi, G. Cui, M. Wang, J. Jin, N. Wei, C. Lu, W. Zhao, J. Sun, Z. Liu, ACS Nano, 14 (2020) 11929-11938.

[131] J. He, A. Bhargav, A. Manthiram, ACS Nano, 15 (2021) 8583-8591.

[132] B. Li, Q. Su, L. Yu, J. Zhang, G. Du, D. Wang, D. Han, M. Zhang, S. Ding, B. Xu, ACS Nano, (2020) 17285−17294.

[133] Y. Li, C. Wang, W. Wang, A.Y.S. Eng, M. Wan, L. Fu, E. Mao, G. Li, J. Tang, Z.W. Seh, Y. Sun, ACS Nano, 14 (2019) 1148-1157.

[134] W. Sun, C. Liu, Y. Li, S. Luo, S. Liu, X. Hong, K. Xie, Y. Liu, X. Tan, C. Zheng, ACS Nano, 13 (2019) 12137-12147.

[135] X. Wu, N. Liu, M. Wang, Y. Qiu, B. Guan, D. Tian, Z. Guo, L. Fan, N. Zhang, ACS Nano, 13 (2019) 13109-13115.

[136] Y. Boyjoo, H. Shi, E. Olsson, Q. Cai, Z.S. Wu, J. Liu, G.Q. Lu, Adv. Energy Mater., 10 (2020) 2000651.

[137] Z. Cheng, H. Pan, J. Chen, X. Meng, R. Wang, Adv. Energy Mater., 9 (2019) 1901609.

[138] X. Huang, J. Tang, B. Luo, R. Knibbe, T. Lin, H. Hu, M. Rana, Y. Hu, X. Zhu, Q. Gu, D. Wang, L. Wang, Adv. Energy Mater., 9 (2019) 1901872.

[139] L. Kong, B.-Q. Li, H.-J. Peng, R. Zhang, J. Xie, J.-Q. Huang, Q. Zhang, Adv. Energy Mater., 8 (2018) 1800849.

[140] Z. Liang, D. Yang, P. Tang, C. Zhang, J. Jacas Biendicho, Y. Zhang, J. Llorca, X. Wang, J. Li, M. Heggen, J. David, R.E. Dunin‐Borkowski, Y. Zhou, J.R. Morante, A. Cabot, J. Arbiol, Adv. Energy Mater., 11 (2020) 2003507.

[141] Y.T. Liu, D.D. Han, L. Wang, G.R. Li, S. Liu, X.P. Gao, Adv. Energy Mater., 9 (2019) 1803477.

[142] D. Luo, G. Li, Y.P. Deng, Z. Zhang, J. Li, R. Liang, M. Li, Y. Jiang, W. Zhang, Y. Liu, W. Lei, A. Yu, Z. Chen, Adv. Energy Mater., 9 (2019) 1900228.

[143] Z. Sun, S. Vijay, H.H. Heenen, A.Y.S. Eng, W. Tu, Y. Zhao, S.W. Koh, P. Gao, Z.W. Seh, K. Chan, H. Li, Adv. Energy Mater., 10 (2020) 1904010.

[144] J. Wang, G. Yang, J. Chen, Y. Liu, Y. Wang, C.Y. Lao, K. Xi, D. Yang, C.J. Harris, W. Yan, S. Ding, R.V. Kumar, Adv. Energy Mater., 9 (2019) 1902001.

[145] Y. Wang, R. Zhang, J. Chen, H. Wu, S. Lu, K. Wang, H. Li, C.J. Harris, K. Xi, R.V. Kumar, S. Ding, Adv. Energy Mater., 9 (2019) 1900953.

[146] Z. Shen, M. Cao, Z. Zhang, J. Pu, C. Zhong, J. Li, H. Ma, F. Li, J. Zhu, F. Pan, H. Zhang, Adv. Funct. Mater., 30 (2019) 1906661.

[147] R. Wang, R. Wu, X. Yan, D. Liu, P. Guo, W. Li, H. Pan, Adv. Funct. Mater., 32 (2022) 2200424.

[148] Q. Yu, Y. Lu, R. Luo, X. Liu, K. Huo, J.-K. Kim, J. He, Y. Luo, Adv. Funct. Mater., 28 (2018) 1804520.

[149] C. Zhang, J.J. Biendicho, T. Zhang, R. Du, J. Li, X. Yang, J. Arbiol, Y. Zhou, J.R. Morante, A. Cabot, Adv. Funct. Mater., 29 (2019) 1903842.

[150] C. Zhang, R. Du, J.J. Biendicho, M. Yi, K. Xiao, D. Yang, T. Zhang, X. Wang, J. Arbiol, J. Llorca, Y. Zhou, J.R. Morante, A. Cabot, Adv. Funct. Mater., 11 (2021) 2100432.

[151] D. Zhang, S. Wang, R. Hu, J. Gu, Y. Cui, B. Li, W. Chen, C. Liu, J. Shang, S. Yang, Adv. Funct. Mater., 30 (2020) 2002471.

[152] H. Zhang, W. Zhao, M. Zou, Y. Wang, Y. Chen, L. Xu, H. Wu, A. Cao, Adv. Funct. Mater., 8 (2018) 1800013.

[153] Y. Zhang, G. Li, J. Wang, G. Cui, X. Wei, L. Shui, K. Kempa, G. Zhou, X. Wang, Z. Chen, Adv. Funct. Mater., 30 (2020) 2001165.

[154] Y. Zhong, D. Chao, S. Deng, J. Zhan, R. Fang, Y. Xia, Y. Wang, X. Wang, X. Xia, J. Tu, Adv. Funct. Mater., 28 (2018) 1706391.

[155] X. Zhu, W. Zhao, Y. Song, Q. Li, F. Ding, J. Sun, L. Zhang, Z. Liu, Adv. Funct. Mater., 8 (2018) 1800201.

[156] L. Kong, X. Chen, B.-Q. Li, H.-J. Peng, J.-Q. Huang, J. Xie, Q. Zhang, Adv. Mater., 30 (2018) 1705219.

[157] D. Luo, C. Li, Y. Zhang, Q. Ma, C. Ma, Y. Nie, M. Li, X. Weng, R. Huang, Y. Zhao, L. Shui, X. Wang, Z. Chen, Adv. Mater., 34 (2022) e2105541.

[158] L. Luo, S.H. Chung, H. Yaghoobnejad Asl, A. Manthiram, Adv. Mater., 30 (2018) e1804149.

[159] Y. Tian, G. Li, Y. Zhang, D. Luo, X. Wang, Y. Zhao, H. Liu, P. Ji, X. Du, J. Li, Z. Chen, Adv. Mater., 32 (2020) e1904876.

[160] L. Wang, W. Hua, X. Wan, Z. Feng, Z. Hu, H. Li, J. Niu, L. Wang, A. Wang, J. Liu, X. Lang, G. Wang, W. Li, Q.H. Yang, W. Wang, Adv. Mater., 34 (2022) e2110279.

[161] H. Xu, Q. Jiang, B. Zhang, C. Chen, Z. Lin, Adv. Mater., 32 (2020) e1906357.

[162] X. Yang, X. Gao, Q. Sun, S.P. Jand, Y. Yu, Y. Zhao, X. Li, K. Adair, L.Y. Kuo, J. Rohrer, J. Liang, X. Lin, M.N. Banis, Y. Hu, H. Zhang, X. Li, R. Li, H. Zhang, P. Kaghazchi, T.K. Sham, X. Sun, Adv. Mater., 31 (2019) e1901220.

[163] Y.T. Liu, S. Liu, G.R. Li, T.Y. Yan, X.P. Gao, Adv. Sci., 7 (2020) 1903693.

[164] J. Wang, H. Yang, Z. Chen, L. Zhang, J. Liu, P. Liang, H. Yang, X. Shen, Z.X. Shen, Adv. Sci., 5 (2018) 1800621.

[165] J. Yu, J. Xiao, A. Li, Z. Yang, L. Zeng, Q. Zhang, Y. Zhu, L. Guo, Angew Chem Int Ed Engl, 59 (2020) 13071-13078.

[166] Y. Yang, Y. Zhong, Q. Shi, Z. Wang, K. Sun, H. Wang, Angew. Chem. Int. Ed., 57 (2018) 15549-15552.

[167] M. Zhao, H.J. Peng, Z.W. Zhang, B.Q. Li, X. Chen, J. Xie, X. Chen, J.Y. Wei, Q. Zhang, J.Q. Huang, Angew. Chem. Int. Ed., 58 (2019) 3779-3783.

[168] S. Ma, L. Wang, Y. Wang, P. Zuo, M. He, H. Zhang, L. Ma, T. Wu, G. Yin, Carbon, 143 (2019) 878-889.

[169] Z. Zhang, S. Basu, P. Zhu, H. Zhang, A. Shao, N. Koratkar, Z. Yang, Carbon, 142 (2019) 32-39.

[170] M. Zhao, B.-Q. Li, X. Chen, J. Xie, H. Yuan, J.-Q. Huang, Chem, 6 (2020) 3297-3311.

[171] G. Li, W. Lei, D. Luo, Y. Deng, Z. Deng, D. Wang, A. Yu, Z. Chen, Energy Environ. Sci. , 11 (2018) 2372-2381.

[172] G. Chen, Y. Li, W. Zhong, F. Zheng, J. Hu, X. Ji, W. Liu, C. Yang, Z. Lin, M. Liu, Energy Storage Mater., 25 (2020) 547-554.

[173] H. Li, S. Ma, H. Cai, H. Zhou, Z. Huang, Z. Hou, J. Wu, W. Yang, H. Yi, C. Fu, Y. Kuang, Energy Storage Mater., 18 (2019) 338-348.

[174] Y. Li, J. Wu, B. Zhang, W. Wang, G. Zhang, Z.W. Seh, N. Zhang, J. Sun, L. Huang, J. Jiang, J. Zhou, Y. Sun, Energy Storage Mater., 30 (2020) 250-259.

[175] Y. Liu, Z. Wei, B. Zhong, H. Wang, L. Xia, T. Zhang, X. Duan, D. Jia, Y. Zhou, X. Huang, Energy Storage Mater., 35 (2021) 12-18.

[176] B. Wang, F. Jin, Y. Xie, H. Luo, F. Wang, T. Ruan, D. Wang, Y. Zhou, S. Dou, Energy Storage Mater., 26 (2020) 433-442.

[177] Y. Wang, R. Zhang, Y.-c. Pang, X. Chen, J. Lang, J. Xu, C. Xiao, H. Li, K. Xi, S. Ding, Energy Storage Mater., 16 (2019) 228-235.

[178] S. Zhang, P. Zhang, R. Hou, B. Li, Y. Zhang, K. Liu, X. Zhang, G. Shao, J. Energy Chem., 47 (2020) 281-290.

[179] L. Luo, S.-H. Chung, A. Manthiram, J. Mater. Chem. A, 6 (2018) 7659-7667.

[180] P. Wang, Z. Zhang, X. Yan, M. Xu, Y. Chen, J. Li, J. Li, K. Zhang, Y. Lai, J. Mater. Chem. A, 6 (2018) 14178-14187.

[181] J. Wu, X. Li, H. Zeng, Y. Xue, F. Chen, Z. Xue, Y. Ye, X. Xie, J. Mater. Chem. A, 7 (2019) 7897-7906.

[182] Q. Pang, C.Y. Kwok, D. Kundu, X. Liang, L.F. Nazar, Joule, 3 (2019) 136-148.

[183] Y. Chen, S. Choi, D. Su, X. Gao, G. Wang, Nano Energy, 47 (2018) 331-339.

[184] L. Du, Q. Wu, L. Yang, X. Wang, R. Che, Z. Lyu, W. Chen, X. Wang, Z. Hu, Nano Energy, 57 (2019) 34-40.

[185] Y. Song, W. Zhao, N. Wei, L. Zhang, F. Ding, Z. Liu, J. Sun, Nano Energy, 53 (2018) 432-439.

[186] S. Wang, J. Liao, X. Yang, J. Liang, Q. Sun, J. Liang, F. Zhao, A. Koo, F. Kong, Y. Yao, X. Gao, M. Wu, S.-Z. Yang, R. Li, X. Sun, Nano Energy, 57 (2019) 230-240.

[187] H. Wu, Y. Li, J. Ren, D. Rao, Q. Zheng, L. Zhou, D. Lin, Nano Energy, 55 (2019) 82-92.

[188] J. Xu, W. Zhang, H. Fan, F. Cheng, D. Su, G. Wang, Nano Energy, 51 (2018) 73-82.

[189] Z. Ye, Y. Jiang, J. Qian, W. Li, T. Feng, L. Li, F. Wu, R. Chen, Nano Energy, 64 (2019) 103965.

[190] J. Zhang, G. Li, Y. Zhang, W. Zhang, X. Wang, Y. Zhao, J. Li, Z. Chen, Nano Energy, 64 (2019) 103905.

[191] L. Ma, H. Lin, W. Zhang, P. Zhao, G. Zhu, Y. Hu, R. Chen, Z. Tie, J. Liu, Z. Jin, Nano Lett., 18 (2018) 7949-7954.

[192] F. Ma, J. Liang, T. Wang, X. Chen, Y. Fan, B. Hultman, H. Xie, J. Han, G. Wu, Q. Li, Nanoscale, 10 (2018) 5634-5641.

[193] R. Luo, Q. Yu, Y. Lu, M. Zhang, T. Peng, H. Yan, X. Liu, J.-K. Kim, Y. Luo, Nanoscale Horiz., 4 (2019) 531-539.

[194] Z.-L. Xu, J.-K. Kim, K. Kang, Nano Today, 19 (2018) 84-107.

[195] E. Cha, M. Patel, S. Bhoyate, V. Prasad, W. Choi, Nanoscale Horiz, 5 (2020) 808-831.

[196] X.Y. Li, S. Feng, C.X. Zhao, Q. Cheng, Z.X. Chen, S.Y. Sun, X. Chen, X.Q. Zhang, B.Q. Li, J.Q. Huang, Q. Zhang, J. Am. Chem. Soc., (2022), 2c04176.

[197] X.Y. Li, S. Feng, M. Zhao, C.X. Zhao, X. Chen, B.Q. Li, J.Q. Huang, Q. Zhang, Angew. Chem. Int. Ed., 61 (2022) e202114671.

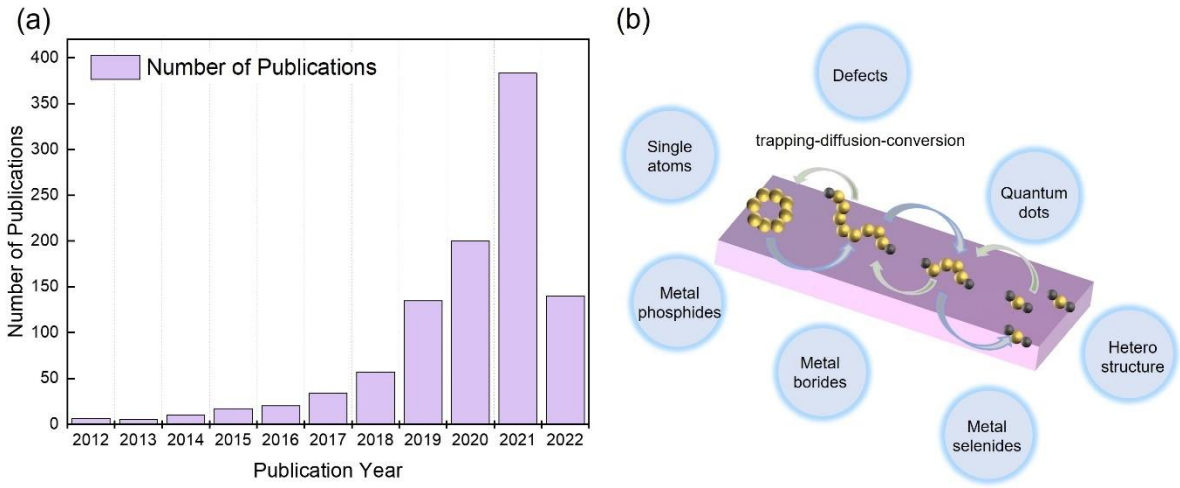

Fig. 1. (a) Number of publications about lithium sulfur battery with catalysts in past decade. (Source: Web of science). (b) Illustration of the emerging catalysts.

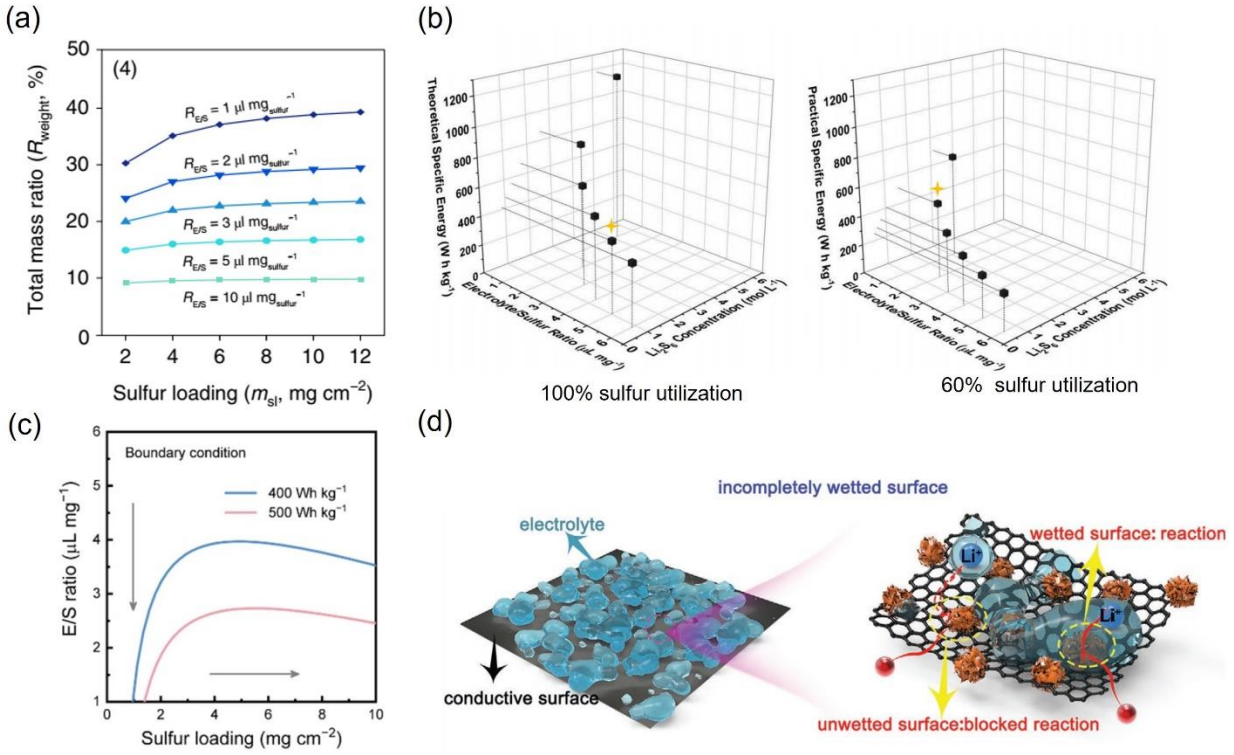

Fig. 2. (a) The relationship of total mass ratio with different E/S ratios and different sulfur loading. Reproduced from Ref. [1] with permission from the Springer Nature; (b) The relationship between the E/S ratio and theoretical specific energy (100% sulfur utilization)/ practical specific energy (60% sulfur utilization). Reproduced from Ref. [30] with permission from Wiley-VCH; (c) The required E/S ratio and sulfur loading using 400 Wh hg^{-1} and 500 Wh hg^{-1} as the boundary condition. Reproduced from Ref. [14] with permission from the American Chemical Society; (d) Schematic illustration of the electrolyte cannot fully wet the conductive surface in lean electrolyte condition. Reproduced from Ref.[36] with permission from Wiley-VCH.

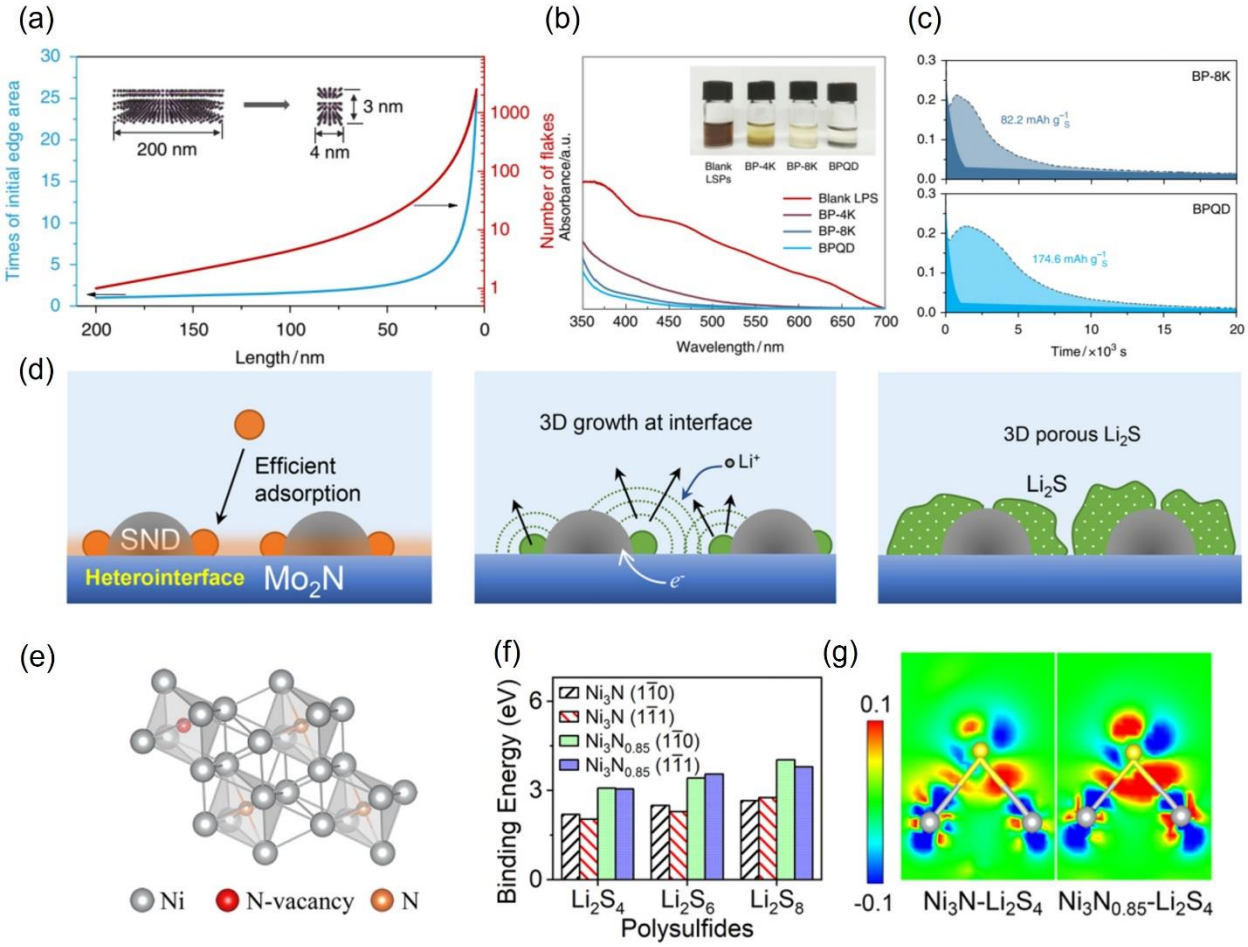

Fig.3. (a) The relationship between black phosphorus size and exposed edge area. (b) Absorption ability comparison of different sizes of black phosphorus. (c) Catalytic ability comparison of different sizes of black phosphorus for Li_2S deposition. Reproduced from Ref.[52] with permission from Springer Nature; (d) Schematic illustration of heterointerface of the SnO_2/Mo_2N favoring Li_2S 3D deposition. Reproduced from Ref.[46] with permission from the American Chemical Society; (e) The structure of Ni_3N with nitrogen vacancies. (f) The binding energy of $Ni_3N_{0.85}$ and Ni_3N with soluble LiPSs. (g) Electron density of Ni-S bonds in $Ni_3N_{0.85}$. Reproduced from Ref.[58] with permission from the American Chemical Society.

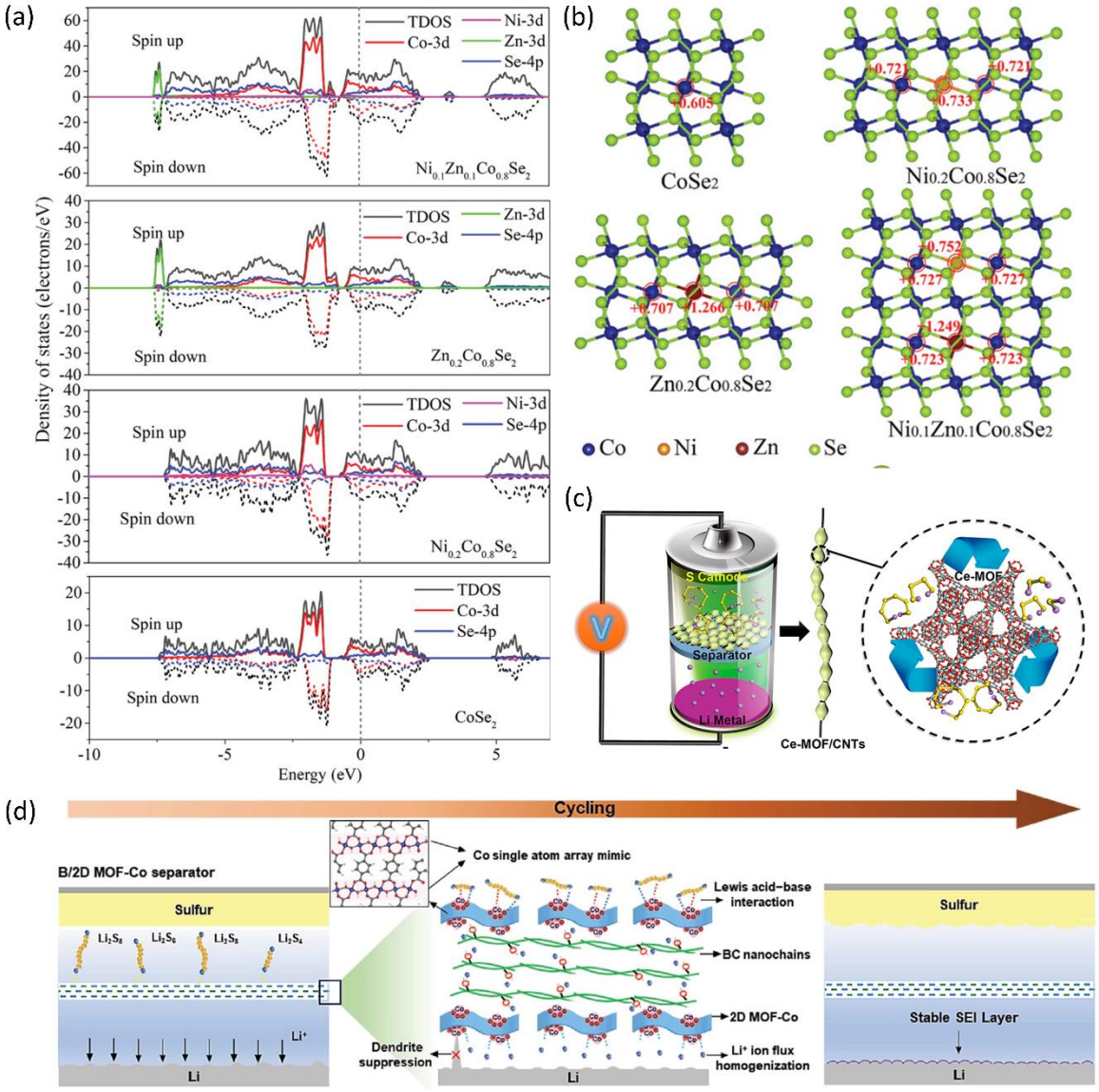

Fig.4. (a) The density of states (DOS) of $CoSe_2$, Zn-doped $CoSe_2$, Ni-doped $CoSe_2$, Zn, Ni-doped $CoSe_2$. (b) The charge number of Co atoms in $CoSe_2$, Zn-doped $CoSe_2$, Ni-doped $CoSe_2$, Zn, Ni-doped $CoSe_2$. Reproduced from Ref.[66] with permission from Wiley-VCH; (c) Schematic illustration of Ce-MoF/CNT modified separator. Reproduced from Ref.[69] with permission from American Chemical Society; (d) Schematic illustration of ultrathin MOF nanosheets with single Co atom array mimics modified separator suppressing shuttle effect and lithium dendrite. Reproduced from Ref.[71] with permission from Wiley-VCH.

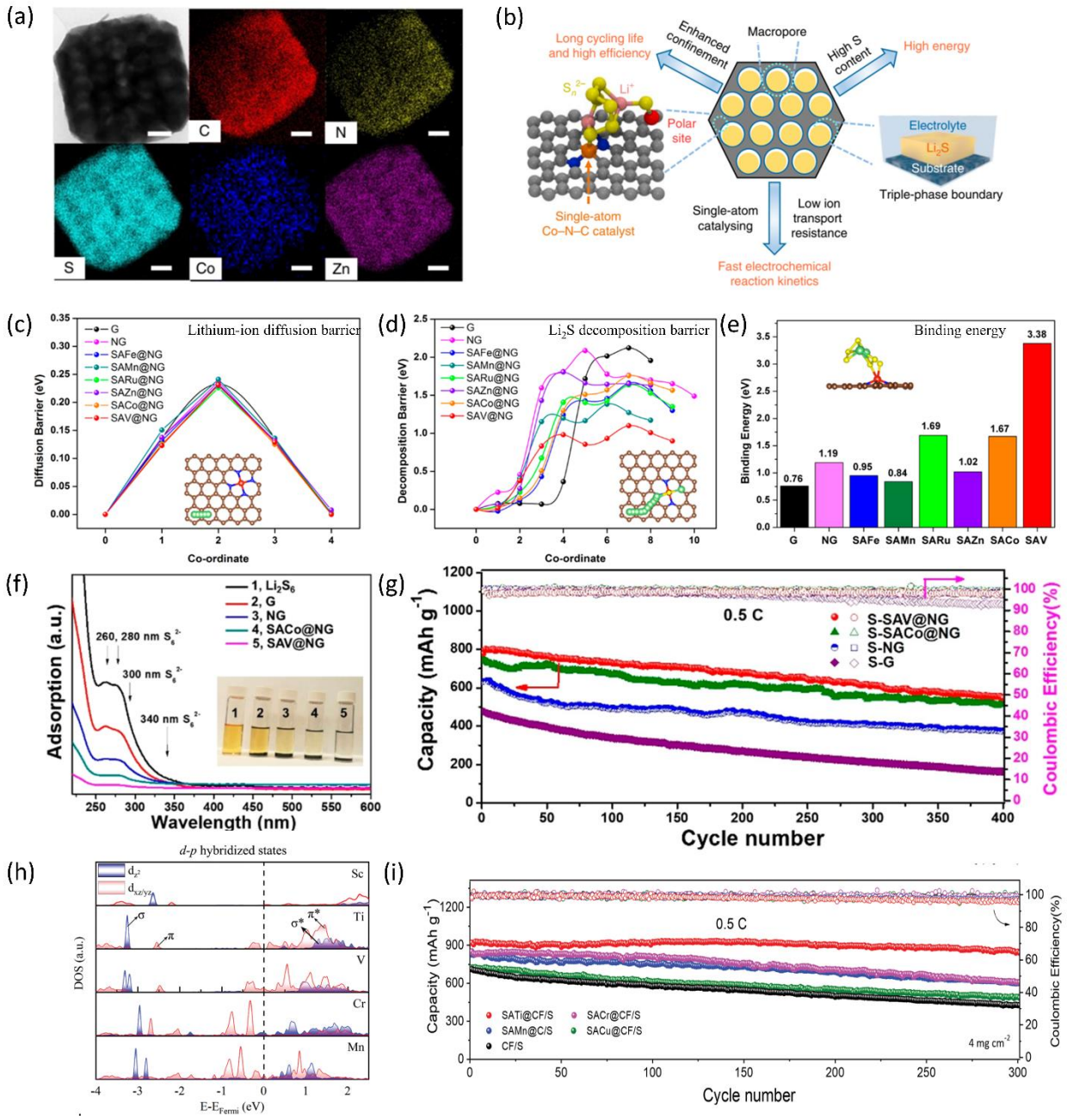

Fig.5. (a) TEM image and EDS mapping of a highly oriented macroporous decorated by ZnS nanoparticles and Co-N-C single atoms, (b) illustration of working mechanism of the structure in (a). Reproduced from Ref.[76] with permission from Springer Nature; DFT calculations of (c) the Li-ion diffusion barrier, (d) the Li_2S decomposition barrier, and (e) the binding energies to Li_2S_6 for different SAC@NG catalysts, (f) comparison of graphene, N-doped graphene (NG), SAV@NG, and SAV@NG absorption ability to Li_2S_6, (g) cyclic performance of S-G, S- NG, S-AV@NG, and S-SACo@NG cathodes. Reproduced from Ref.[79] with permission from American Chemical Society. (h) d-p orbital hybridization states of Se, Ti, V, Cr, Mn, (i) cyclic performance of SATi@CF/S, SACr@CF/S, SAMn@CF/S, SACu@CF/S and CF/S at 0.5C. Reproduced from Ref.[77] with permission from Wiley-VCH.

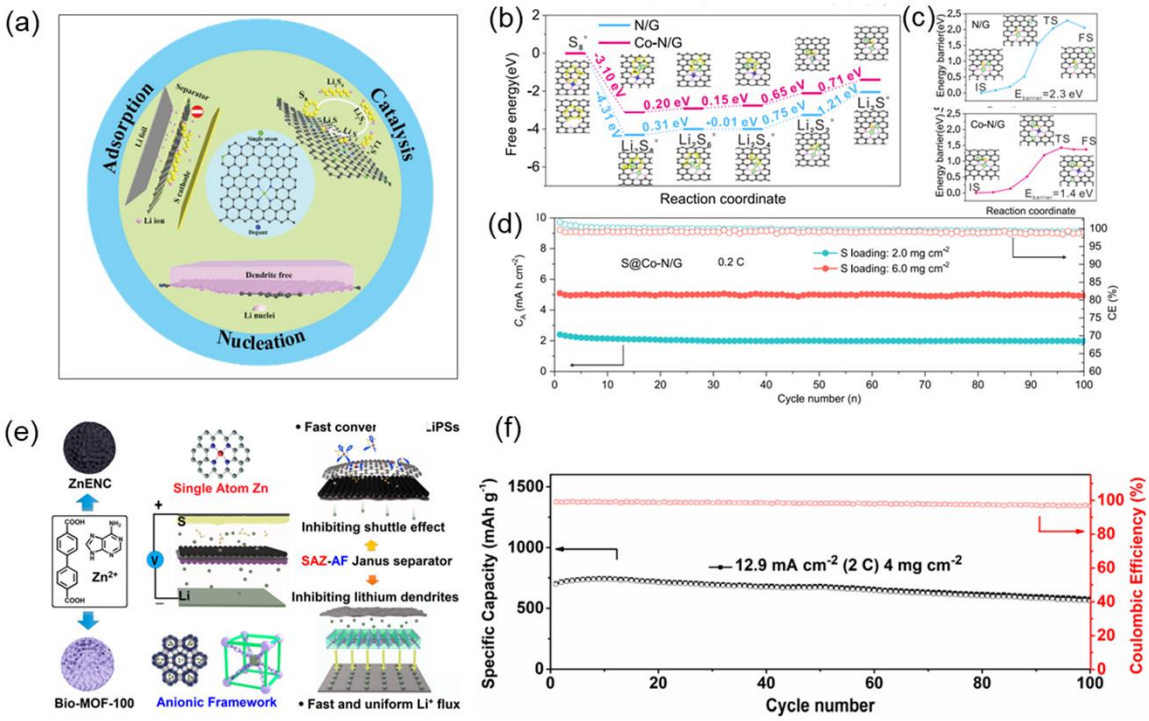

Fig.6. (a) Schematic illustration of single-atom catalysts applied in S cathode, Li anode, and separators. Reproduced from Ref.[81] with permission from the Wiley-VCH; Comparison of (b) free energies for LiPS reduction and (c) Li_2S decomposition barrier on N/G substrates and Co-N/G substrates, (d) cyclic performance of S@Co-N/G at 0.2 C for 100 cycles. Reproduced from Ref.[84] with permission from the American Chemical Society; (e) schematic illustration of a dual-functional SAZ-AF Janus separator, (f) cycling performance of the cell at 2C with m_{sl} of 4 mg cm^{-2}. Reproduced from Ref.[88] with permission from the American Chemical Society.

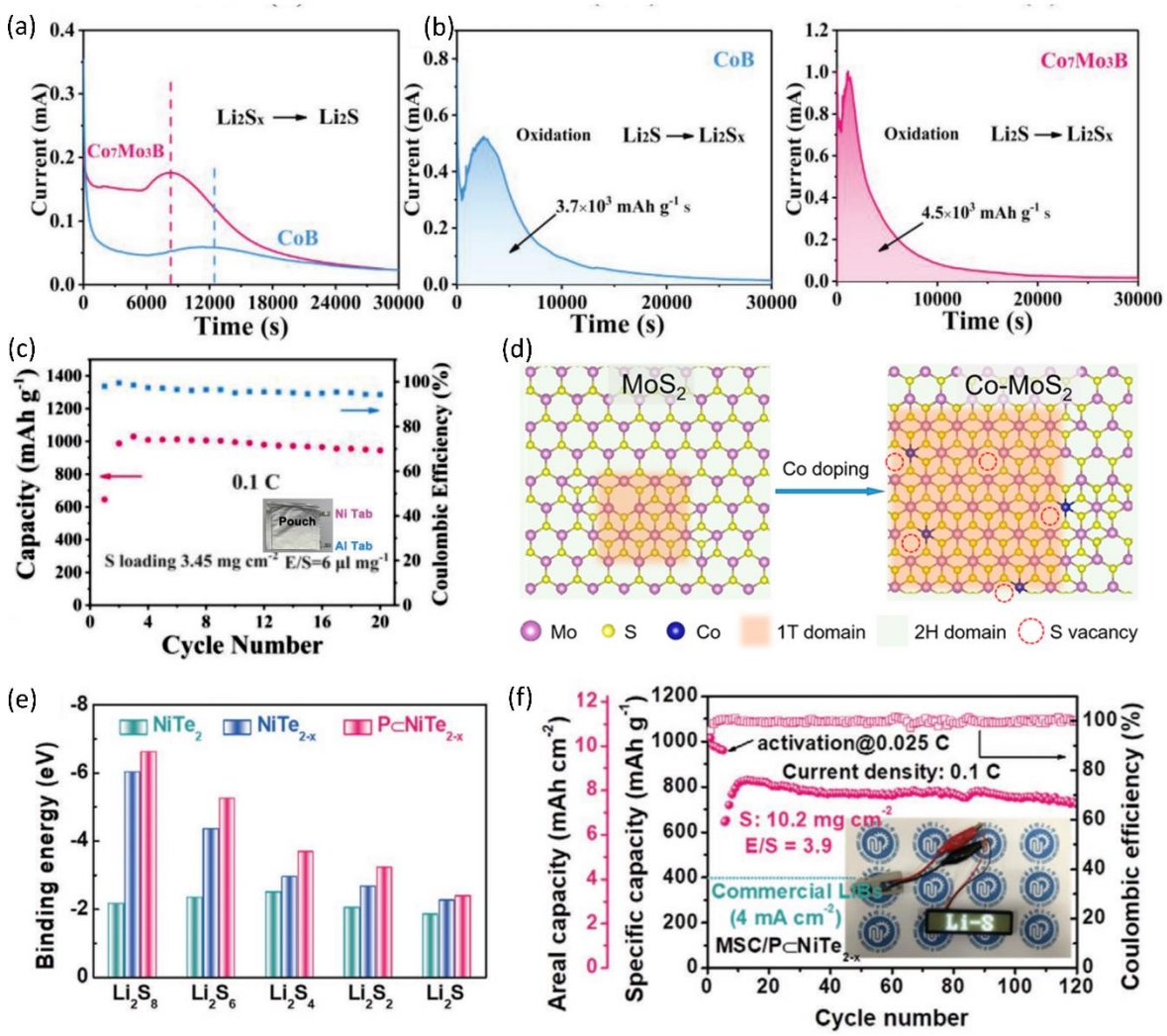

Fig.7. (a) The comparison of the process of Li_2S_x reduction to Li_2S using Co_7Mo_3B and CoB as catalysts. (b) The comparison of the capacity of Li_2S oxidation to Li_2S_x using Co_7Mo_3B and CoB as catalysts. (c) Cycling performance and Coulombic efficiency of pouch cell at 0.1 C with m_{sl} of 3.45 mg cm^{-2} and E/S ratio of 6 μl mg^{-1}. Reproduced from Ref. [93] with permission from Wiley-VCH. (d) Schematic illustration of 1H MoS_2 and S vacancy formation after Co doping into 2H MoS_2. Reproduced from Ref. [94] with permission from the American Chemical Society. (e) The comparison of the binding energy of $NiTe_{2-x}$ and $NiTe_2$, $P⊂NiTe_{2-x}$ to Li_2S_8, Li_2S_6, Li_2S_4, Li_2S_2 and Li_2S. (f) Cycling performance and Coulombic efficiency of cell at 0.1 C with m_{sl} of 10.2 mg cm^{-2} and E/S ratio of 3.9 μl mg^{-1}. Reproduced from Ref.[104] with permission from Wiley-VCH.

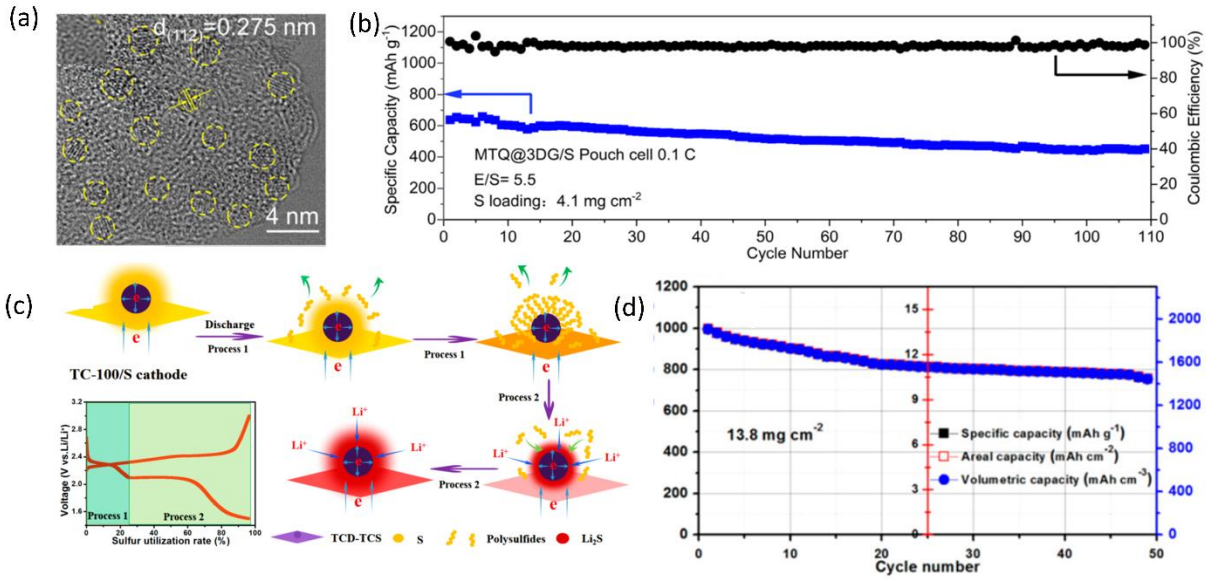

Fig.8. (a) TEM images of 1T'-$MoTe_2$ QDs dispersed on graphene. (b) Cycling performance of the cell at 0.1 C for 110cycles with m_{sl} of 4.1 mg cm^{-2} and E/S ratio of 5.5 µl mg^{-1}. Reproduced from [108] with permission from the American Chemical Society; (c) Schematic illustration of MXene nanodots improving reaction kinetic and suppressing shuttle effect. (d) Cycling performance of cell at 0.05C for 50 cycles with m_{sl} of 13.8 mg cm^{-2} and E/S ratio of 10 µL mg^{-1}. Reproduced from [54] with permission from the American Chemical Society.

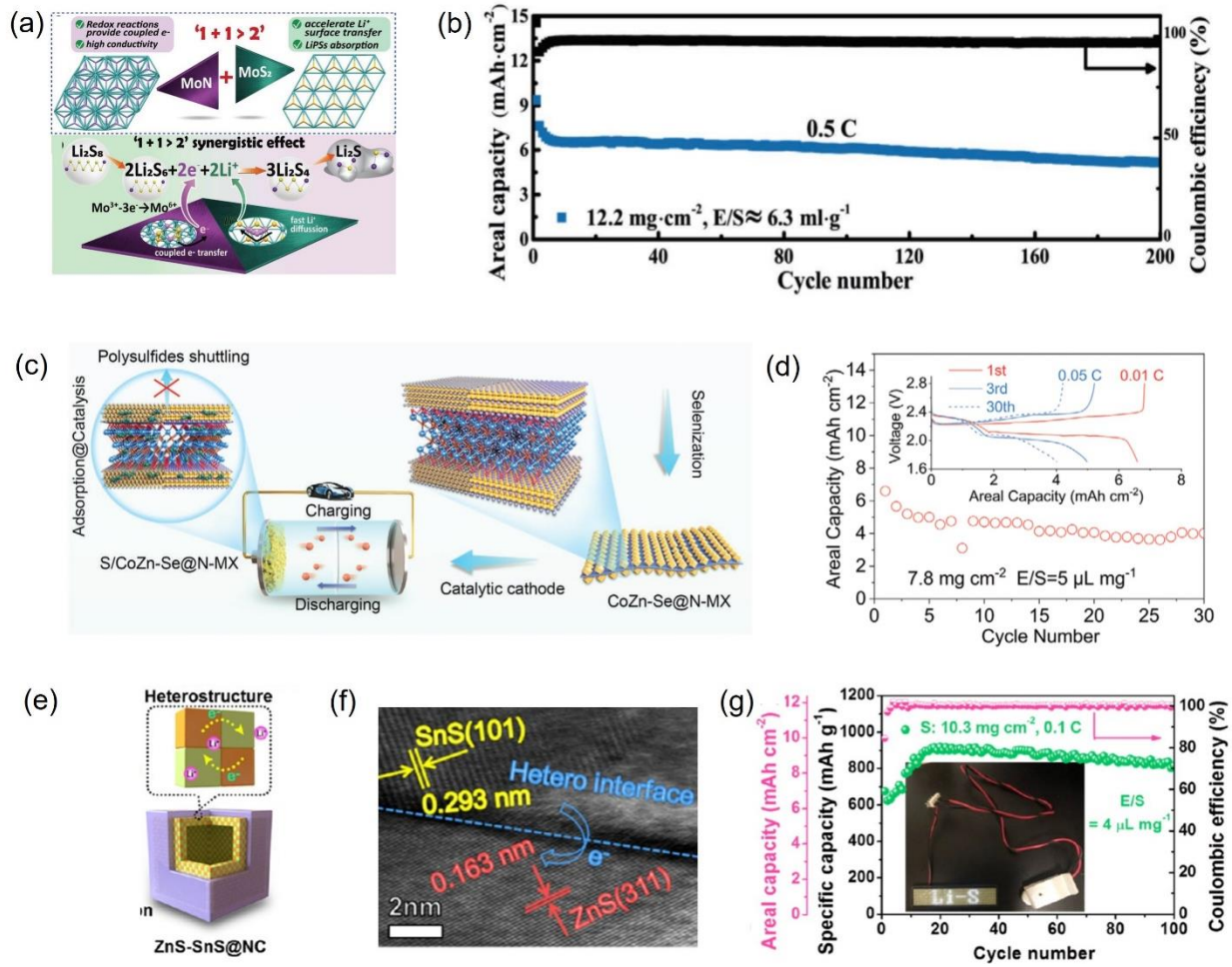

Fig.9. (a) MoN/MoS_2 heterostructure. (b) Cycling performance and Coulombic efficiency of the cell at 0.5 C for 200 cycles with a m_{sl} of 12.2 mg cm^{-2} and E/S ratio of 6.3 ml g^{-1}. Reproduced from Ref. [75] with permission from the Wiley-VCH; (c) working mechanism of S/CoZn-Se@N-MX to improve reaction kinetic and suppress shuttle effect. (d) Cycling performance of cell at 0.05C for 30 cycles with m_{sl} of 7.8 mg cm^{-2} and E/S ratio of 5 μl mg^{-1}. Reproduced from Ref. [115] with permission from the Wiley-VCH; (e) ZnS-SnS nanobox coated by a N-doped carbon shell. (f) TEM image of the ZnS-SnS heterointerface. (g) Cycling performance of the cell at 0.1 C for 100 cycles with m_{sl} of 10.3 mg cm^{-2} and an E/S ratio of 4 μl mg^{-1}. Reproduced from Ref. [112] with permission from the American Chemical Society.

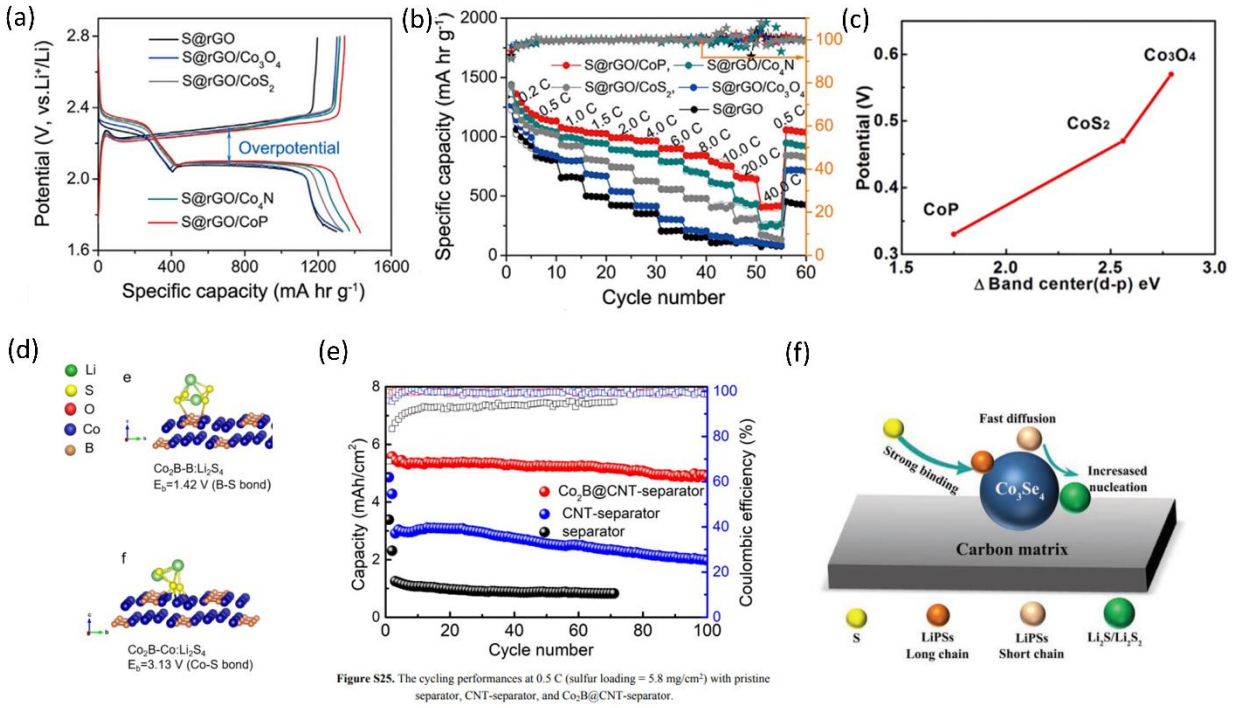

Fig. 10. (a)The specific capacity and overpotential of different Co-based components as cathode. (b)The rate performance of different Co-based components as cathode. (c)The relationship between overpotential and band center(d-p). Reproduced from Ref.[9] with permission from the Elsevier. (d) Schematic diagram of Co_2B anchoring Li_2S_4 via Co-S and B-S bonds. (e) The cycling performance of cells using Co2B@CNT-separator, CNT-separator and general separator with m_{sl}= 5.8 mg cm^{-2} at 0.5C. Reproduced from Ref.[119] with permission from the American Chemical Society. (f) Schematic illustration of the ability of Co_3Se_4 to anchor LIPSs and catalyze LiPSs conversion. Reproduced from Ref. [126] with permission from the Wiley-VCH.

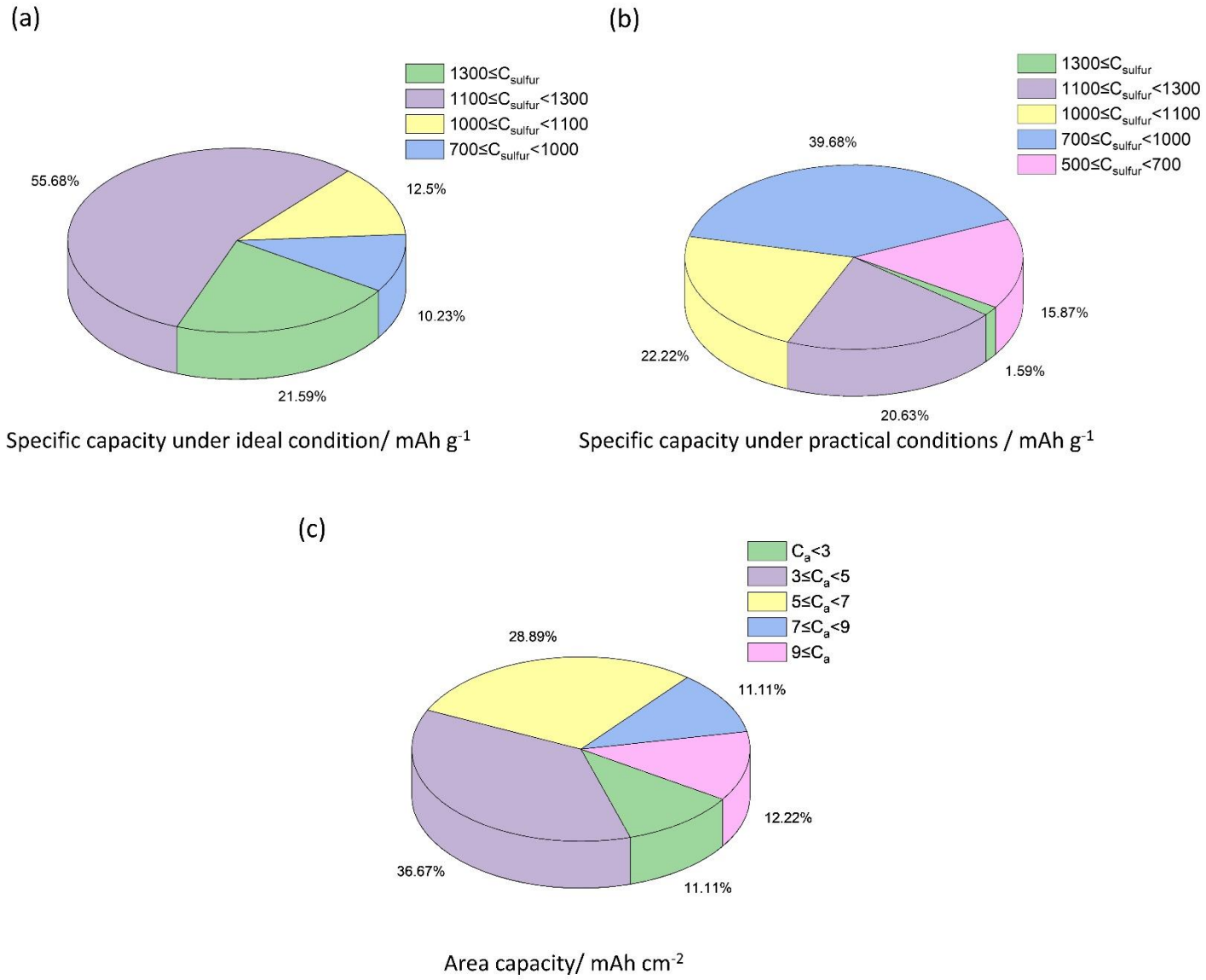

Fig.11. Statistical analysis of LSB performance on (a) specific capacities under ideal condition, (b) specific capacities and (c) area capacities under practical conditions.

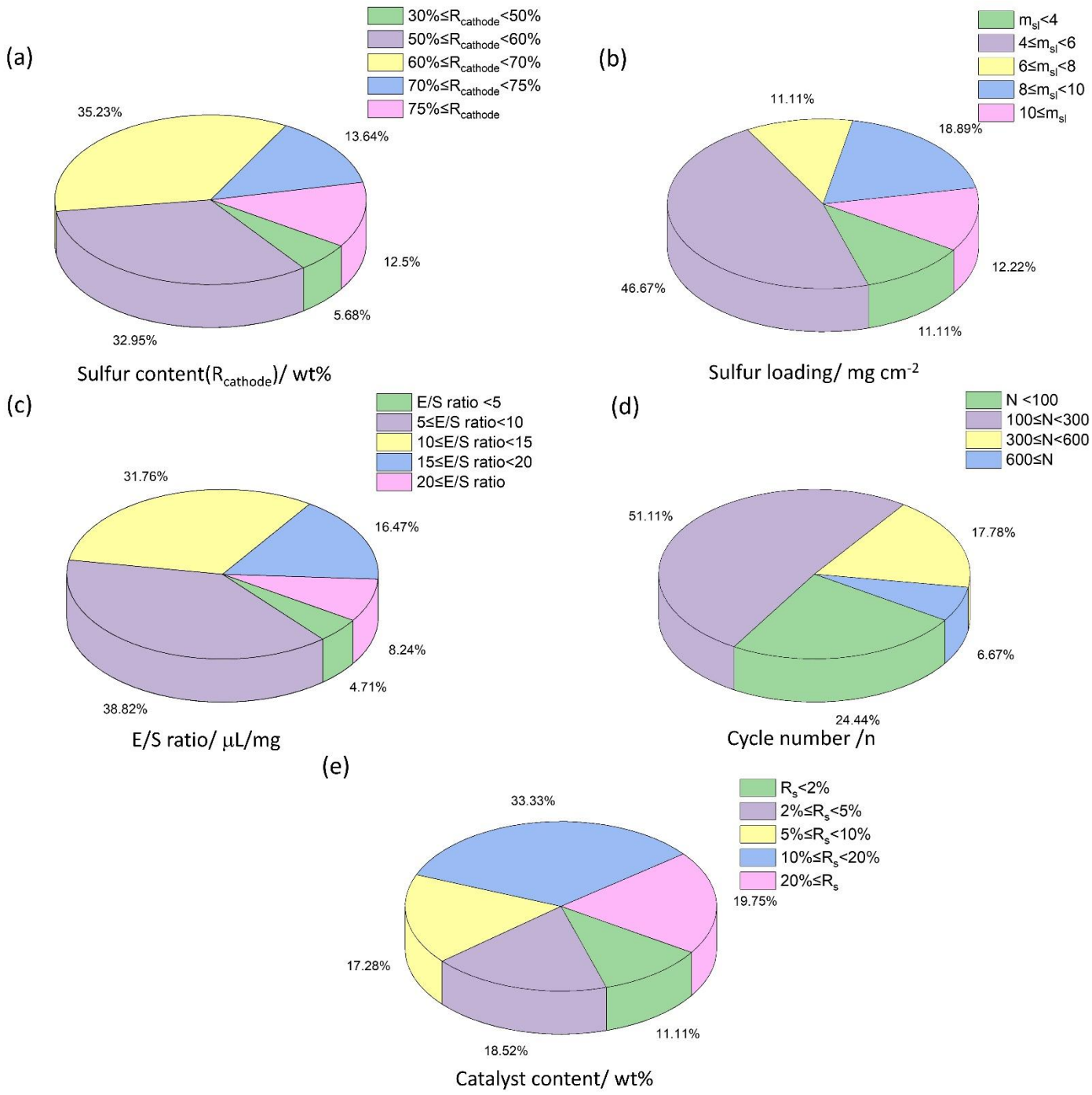

Fig.12. Statistical analysis of publications on (a) sulfur content, (b) sulfur loading, (c) E/S ratio, (d) cycle number, and (e) catalyst content.